Politecnico di Torino

Politecnico di Torino

Master of science degree in
Communications Engineering

Next-generation optical metro+access network using coherent detection

A.Y. 2024/25

Supervisors

Prof. Roberto GAUDINO

Dr. Dario PILORI

Candidate

Davide CASOLA

Summary

In today's digitalized world, the demand for data transmission continues to grow, pushing network capacities to their limits. While coherent transceivers effectively meet user demands in long-haul transmissions, new solutions are required for metro access networks.

This challenge arises due to the different detection technologies used in metro-access passive optical networks (**PONs**), specifically Intensity Modulation Direct-Detection (**IMDD**). From a capacity perspective, IMDD is significantly limited compared to coherent detection, as it does not support advanced modulation formats that provide higher spectral efficiency. On the other hand, implementing coherent transmission is more complex and costly, making it unsuitable for the PON context.

The proposed solution is a simplified version of the coherent detection technology used in long-haul transmissions, optimized for metro access PONs (referred to as **Lite Coherent**).

This project primarily focuses on implementing a digital signal processing (**DSP**) coherent receiver capable of handling typical PON impairments, such as phase noise, frequency offset, and others.

To enhance robustness in the developed optical system, the project explores an alternative modulation scheme: Differential Quadrature Phase Shift Keying (**DQPSK**), as opposed to the conventional Quadrature Phase Shift Keying (**QPSK**).

Through comprehensive performance analysis, the results demonstrate that DQPSK is a viable modulation option for access network scenarios.

Table of Contents

1 Introduction 1
- 1.1 Context . . . 2
- 1.2 Goal of the Project . . . 3
- 1.3 Structure of the Document . . . 3

2 Analyzed Modulations and Simulator Structure 5
- 2.1 Modulations . . . 5
  - 2.1.1 Quadrature Phase Shift Keying . . . 6
  - 2.1.2 Differential Quadrature Phase Shift Keying . . . 7
  - 2.1.3 QPSK vs DQPSK . . . 8
- 2.2 Simulation Setup . . . 10
  - 2.2.1 Transmitter . . . 10
  - 2.2.2 Channel . . . 11
  - 2.2.3 Coherent DSP Receiver . . . 12

3 System Impact of Laser Phase Noise 16
- 3.1 Definition . . . 16
- 3.2 Carrier Phase Estimation Algorithm . . . 17
- 3.3 Results . . . 18
  - 3.3.1 Comparison with Analytic Curve (QPSK) . . . 18
  - 3.3.2 Comparison with Analytic Curve (DQPSK) . . . 21
  - 3.3.3 Discussion and Comparison . . . 24

4 System Impact of Frequency Offset 27
- 4.1 Definition . . . 27
- 4.2 Frequency Offset Compensation Algorithms . . . 28
  - 4.2.1 Differential Phase-Based Method . . . 28
  - 4.2.2 Spectral Method . . . 28
  - 4.2.3 FFT-Based Method . . . 29
- 4.3 Results . . . 30
  - 4.3.1 FOC Algorithms Comparison . . . 31

4.3.2 Comparison with Analytic Curve (QPSK) 38
4.3.3 Comparison with Analytic Curve (DQPSK) 43
4.3.4 Extreme Scenarios 48
4.3.5 Convergence Times 54

5 Conclusions and Future Work 57

List of Tables 59

List of Figures 60

Bibliography 64

Chapter 1

Introduction

Passive Optical Networks (**PONs**) are fiber-optic communication systems that provide **high-speed** broadband access using passive splitters in the distribution network. Traditional solutions rely on Intensity-Modulation Direct-Detection (**IMDD**) techniques, such as Time-Division Multiplexing PONs (**TDM-PONs**), which have been widely deployed due to their cost-effectiveness and simplicity [1].

However, the increasing demand for higher data rates, lower latency, and improved spectral efficiency has driven the development of advanced solutions, including **Coherent PONs** and more powerful transceivers. These technologies leverage digital signal processing (**DSP**) and coherent detection to extend reach, increase capacity, and enhance resilience to fiber impairments [2].

A critical trade-off exists between performance and cost. While coherent solutions offer superior transmission quality, they introduce higher system complexity. To address this, **Lite Coherent** DSP receivers have been proposed as a cost-effective alternative, balancing performance improvements with reduced power consumption and hardware requirements.

Efforts to reduce costs focus on optimizing key components, such as employing cost-effective lasers, simplifying DSP receiver architectures, and minimizing power consumption. These optimizations make PON deployments more economically viable and allow for broader adoption, particularly in challenging environments with extreme climatic conditions or rural deployments [3].

1.1 Context

In the metro segment, coherent PONs are spreading very rapidly, since in central offices (**CO**) the communication systems can be accurately managed, monitoring environmental parameters, such as temperature and humidity, which affect laser stability and performance. In recent years, given the bandwidth and dispersion limitations of IMDD, some novel coherent PON architectures were proposed, capable of reaching more than 50 Gbps both upstream and downstream, in a cost-effective way. The following examples can be applied in both metro and access scenarios.

J. Zhou et al. (Huawei)[4] achieved to experimentally demonstrate the first real-time TFDMA-based coherent PON using an ultra simple transceiver at the Optical Network Unit (**ONU**) and a full-coherent transceiver at the Optical Line Terminal (**OLT**). In addition, high-precision DSP-aided frequency locking makes the cost-effective distributed feedback (**DFB**) laser feasible for the ultra-simple coherent transceiver for ONU. Finally, continuous-mode and burst-mode DSP algorithms for processing downstream and upstream signals in TFDMA-based coherent PON, respectively, were implemented.

Another two interesting solutions were introduced by H. Zhang et al. (Cablelabs)[5]. One features time-division multiplexing (**TDM**) with three modulation formats (**DP-QPSK, DP-16QAM, DP-64QAM**) for both downstream and upstream transmission, and the other uses optical frequency comb-based multi-wavelength source for downstream broadcasting and TDM burst with three modulation formats for upstream.

A third architecture is suggested by V. Houtsma and D. van Veen (Nokia)[6], exploiting the already existing IMDD technology used in Data Center, where Data Rates are in the order of hundreds of Gbps. This solution, unfortunately, can be applied only in the access scenario, since IMDD with such high data rates is limited to about 20 km. Potentially, this is the most cost-effective solution because it simply recycles out-of-date components from data centers.

1.2 Goal of the Project

Main focus of this research is to develop a low-complexity DSP receiver and to analyze how different modulation formats react. The considered modulation formats are Dual-Polarization Quadrature Phase Shift Keying (**DP-QPSK**) and Dual-Polarization Differential Quadrature Phase Shift Keying (**DP-DQPSK**). The system is designed for optical access/metro networks.

At the DSP input, the received signal is mainly affected by laser phase noise (transmitter laser and local oscillator), frequency offset between laser and local oscillator (**LO**), and fiber impairments: dispersion, attenuation and birefringence. Also, the signal is passed through an AWGN channel, as lumped noise source.

Regarding DSP structure, only the needed algorithms for PON scenario are implemented such as: Dispersion Compensation, Multi-Input Multi-Output Constant Modulus Algorithm Feed Forward Equalizer (**MIMO CMA FFE**), Frequency Offset Compensation (**FOC**), Polarization Framing, Carrier Phase Estimation (**CPE**) and Hard-Decision (**HD**) Decoding (FEC is not considered in this work).

Throughout the research, differential modulation (**DP-DQPSK**) has been proven to be a very valid modulation format, above all in PON scenarios where DFB lasers have much larger linewidth than external cavity laser (**ECL**) lasers, typically adopted in coherent long-haul systems. Because of this reason, a strong laser phase noise is considered, affecting performances. In this context, DQPSK has shown a very high level of robustness, in terms of BER penalties and Non-Data-Aided (**NDA**) equalization and compensation techniques implemented.

1.3 Structure of the Document

After the Introduction, where the context of PONs and the main aim of this project are described, the thesis is divided into 4 chapters.

Chapter 2 is split in two parts. The first one shows the considered modulation formats (QPSK & DQPSK), showing the constellation diagrams with the corresponding mapping schemes. In the second part, the simulator structure is represented, focusing primarily on the DSP receiver.

In Chapter 3, first preliminary simulation results are displayed. They are obtained considering only Laser Phase Noise and zero frequency offset. Also, in the first two sections, laser phase noise is defined and Carrier Phase Estimation (CPE)

algorithm is briefly explained.

In Chapter 4, Frequency Offset is added into the simulation framework. So, first, the implemented FOC algorithms are described, then results are shown in terms of BER vs SNR, BER penalties and required SNR. In Extreme Scenarios, QPSK & DQPSK are compared under high phase noise and high frequency offset conditions. Finally, in Convergence Times, the two modulation formats are studied, analyzing the preamble needed to have stable data processing.

In Chapter 5, final conclusions are drawn remarking the major results about DQPSK and further research studies are proposed.

Chapter 2

Analyzed Modulations and Simulator Structure

2.1 Modulations

In this project, the system under test (**SUT**) is a coherent DSP receiver (Section 2.2.3), enhanced for access/metro optical networks. The main requirement is to build a low-complexity receiver able to cope with short-reach fiber impairments (e.g. dispersion, birefringence) and laser non-idealities (i.e. phase noise, frequency offset), taking in mind to impact network operator companies as little as possible both economically and energetically.

In order to possibly further streamline the whole SUT two different **phase shift keying** modulations are considered: Quadrature Phase Shift Keying (**QPSK**) and Differential Quadrature Phase Shift Keying (**DQPSK**).

2.1.1 Quadrature Phase Shift Keying

QPSK is a digital modulation format where each two bits, of a transmitted data sequence, are encoded to a given phase shift of the carrier signal, following the corresponding map:

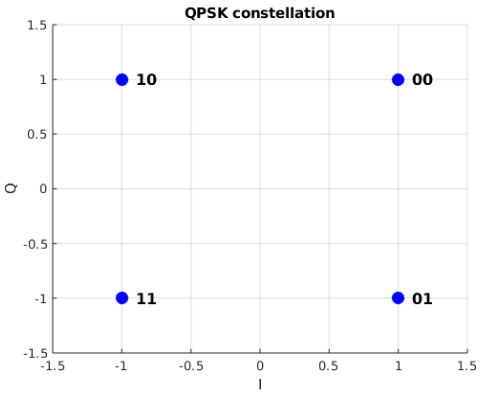

Figure 2.1: QPSK Constellation

Bits	ϕ
00	$\frac{\pi}{4}$
10	$\frac{3\pi}{4}$
11	$\frac{5\pi}{4}$
01	$\frac{7\pi}{4}$

Table 2.1: Symbol Mapping. ϕ is expressed in radiants

$$\tilde{s}_{TX}[n] = \sqrt{E_{symb}} \cdot e^{j\phi[n]} = \sqrt{E_{symb}} \cdot (\cos(\phi[n]) + j\sin(\phi[n]))$$

where:

- $\tilde{s}_{TX}[n]$ is the complex envelope of transmitted signal at the symbol instant n=T_{symb}, $2T_{symb}$, ... ;
- E_{symb} is the symbol energy;
- $\phi[n]$ is the modulated phase of the symbol at the instant $n \cdot T_{symb}$

2.1.2 Differential Quadrature Phase Shift Keying

DQPSK is a digital modulation very similar to QPSK (same constellation points), but conceptually different. Here, the data is encoded in phase differences between successive signal transmissions as opposed to absolute phase encoding (QPSK) following the corresponding map:

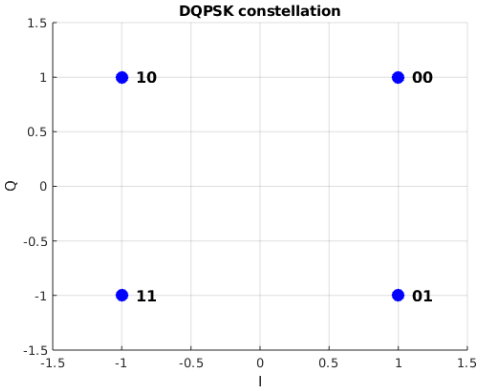

Figure 2.2: DQPSK Constellation

Bits	$\Delta\phi$
00	0
10	$\frac{\pi}{2}$
11	π
01	$\frac{3\pi}{2}$

Table 2.2: Symbol Mapping. $\Delta\phi$ is expressed in radiants

$$\tilde{s}_{TX}[n] = \sqrt{E_{symb}} \cdot e^{j\phi[n]} = \sqrt{E_{symb}} \cdot (\cos(\phi[n]) + j\sin(\phi[n]))$$

where:

- $\tilde{s}_{TX}[n]$ is the complex envelope of transmitted signal at the symbol instant n=T_{symb}, $2T_{symb}$, ... ;
- E_{symb} is the symbol energy;
- $\phi[n] = \phi[n-1] + \Delta\phi[n]$

Equivalently,

$$\tilde{s}_{TX}[n] = \sqrt{E_{symb}} \cdot e^{j\phi[n]} = \tilde{s}_{TX}[n-1] \cdot e^{j\Delta\phi}$$

2.1.3 QPSK vs DQPSK

The DQPSK modulation/demodulation has an intrinsic advantage with respect to QPSK. In a realistic scenario, the transmitter (Section 2.2.1), which generates the optical signal, impacts it introducing phase noise proportional to its linewidth ($\Delta\nu$). Consequently, it is needed a carrier phase estimation stage (CPE).
In **CPE** non-linear operations are applied to the signal. Specifically, to remove the modulation encoding and extract the carrier phase information, the M-PSK sequence (where M denotes the modulation order) is raised to the Mth power [7]. This happens to introduce a phase ambiguity of ± 90° and 180° in the phase estimate. Consequently, there is not an absolute estimate of the carrier phase for demodulation. Although this result deeply impacts QPSK performances, it does not affect DQPSK at all. DQPSK does not depend on an absolute phase reference. Instead, it encodes information in phase transitions. The receiver compares the phase of each symbol to the previous one, rather than trying to determine its absolute phase. Since the receiver only detects changes in phase, any ambiguity (e.g. ± 90° or 180°) does not affect the decoded bits. Thus, the received signal is demodulated and detected to one of the 4 possible transmitted phases. Furthermore, the detector is a relatively simple phase comparator that compares the phases of the demodulated signal over two consecutive intervals to extract the information.
On one hand, the coherent demodulation of QPSK is more susceptible to phase noise, particularly in the form of cycle slips. A cycle slip occurs when phase noise accumulates beyond the ability of the CPE algorithm to track it correctly, resulting in a sudden, incorrect phase shift. Precisely, the implemented CPE algorithm has a $[-\frac{\pi}{4}, \frac{\pi}{4}]$ phase estimation range. This can lead to symbol errors and increased bit error rates (BER). Since QPSK relies on absolute phase reference, phase estimation errors caused by cycle slips can have severe consequences on system performance. In contrast, DQPSK is inherently more robust against cycle slips because it operates differentially. Even if a cycle slip occurs, the relative phase differences between symbols remain largely unaffected, preventing catastrophic error propagation.
On the other hand, the coherent demodulation of DQPSK can cause an higher probability of error than the error probability derived for absolute phase encoding. With differentially encoded PSK, an error in one detected phase can propagate to the next symbol. Therefore, the probability of error in differentially encoded M-ary PSK is approximately twice the probability of error for M-ary PSK with absolute phase encoding [8].

In Figure 2.3, it can be clearly seen the intrinsic penalty of about 3 dB of DQPSK with respect to QPSK. Besides, on the y axis the SNR values correspond to an AWGN channel through which the signal is propagated. It is added since noise sources, such as EDFA amplifiers, are not considered in the simulator. In Figure 2.3, the curves are compared in an ideal scenario, so no phase noise is present.

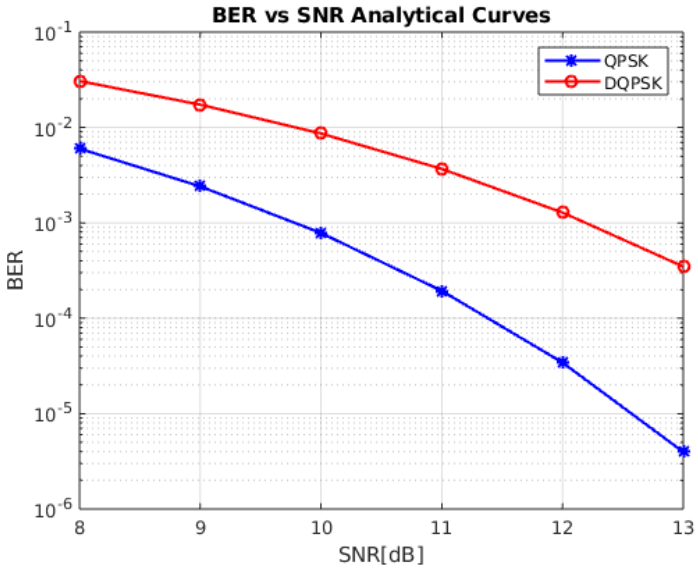

Figure 2.3: Comparison of BER vs SNR Analytical Curves between QPSK and DQPSK

2.2 Simulation Setup

The implemented simulator has a very complex structure. In order to have a more clear and effective description, it is divided in macro blocks: **Transmitter**, **Channel**, **Coherent DSP Receiver**. Each block is defined in the following sections. This paradigm was also adopted in the simulator code, to make the system modular (Object Oriented - MATLAB).

2.2.1 Transmitter

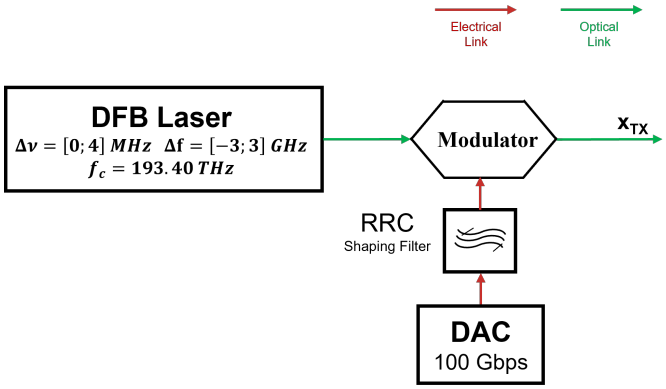

Figure 2.4: Transmitter Block with electrical links (red) and optical links (green)

In Figure 2.4, a high level schematic of the transmitter is shown. Beginning from the optical source, a Distributed FeedBack (DFB) laser has been chosen, characterized by a **linewidth** $\Delta\nu = [1; 4]$ MHz and a **frequency offset** $\Delta f = [-3; 3]$ GHz, very typical of lasers used in PON. Also, the **carrier frequency** has been set at $f_c = 193.40$ THz, exactly at the center of the **C-band**. Regarding the electrical signal , it is a sequence of symbols generated at a rate of 25 GBaud (100 Gbps), then passed through a root raised cosine (**RRC**) shaping filter with an oversampling factor of 2 SpS (Samples per Symbol). In the modulator block, the raw optical signal is modulated according to the chosen modulation (**QPSK** or **DQPSK**) and the electrical signal, carrying the information data. Now, the optical signal (x_{TX}) is launched at the fixed power of 1 mW (0 dBm).

2.2.2 Channel

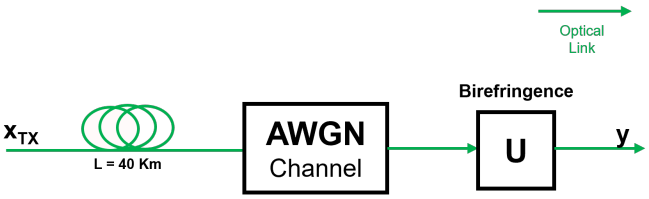

Figure 2.5: Channel Block with electrical links (red) and optical links (green)

Once x_{TX} has been launched, it is propagated through a simulated Single Mode Fiber (**SMF**) span of length 40 km, average value in the metro/access PON. To be mentioned that among the impairments, non-linearities have not been considered, because in short-reach connections they are usually negligible due to low power values. So, only attenuation ($\alpha_{dB} = 0.2$ dB) and Chromatic Dispersion (**CD**:$D = 16.686 \cdot 10^{-6}$ s/m^2) are included in the simulation. Then, since there are no ASE noise sources (no amplifiers), for the sake of completeness, an AWGN channel (**Additive White Gaussian Noise**) is added in order to test the system under different levels of noise ([8;13] dB). To make the system more realistic, a random unitary 2x2 matrix (double polarization) is inserted to simulate the birefringence effect, due to the physical imperfections of optical fibers.

2.2.3 Coherent DSP Receiver

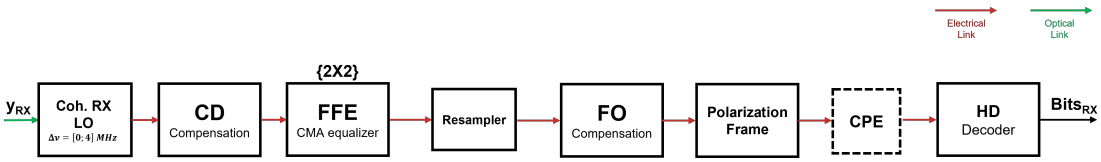

Figure 2.6: Receiver Block with electrical links (red) and optical links (green)

When y_{RX} is received, it is detected through a local oscillator (**LO**) in order to be converted to electric domain. Now, the signal can be processed in order to recover the transmitted one, with as much accuracy as possible [9]-[10].

Chromatic Dispersion Compensation

Along the electrical DSP receiver, first, the chromatic dispersion is compensated. This is done simply passing the received signal through an all-pass filter, which has the transfer function dependent on the central frequency of the signal ($f_c = 193.40$ THz) and on the cumulated dispersion, directly proportional to the span length (40 km).

$$H[n] = e^{-1j\pi \cdot c_0 \cdot CD \cdot (n\frac{f_s}{L_{filt} \cdot f_c})^2} \quad \text{where } n \in [-\frac{L_{filt}}{2}, \frac{L_{filt}}{2} - 1]$$

where:

- c_0 is the speed of light ($3 \cdot 10^8\, m/s$);
- CD is the cumulated dispersion, computed as follow: $CD = D \cdot L_{span}$ [s/m]
- L_{filt} is the filter length
- f_s is the sampling frequency ($f_s = 2R_s = 50$ GBaud)
- f_c is the signal central frequency (193.4 THz)

Adaptive Equalizer

Then, an adaptive feed-forward equalizer (**FFE**) is inserted to deal with polarization mode dispersion (PMD) and recover the transmitted modulation constellation. In particular, the implemented equalizer is a fully blind (no pilots) Constant Modulus Equalizer (**CMA**), so it forces each sample to lie on a circle of fixed radius ($P_{QPSK/DQPSK} = 2$), adapting the transfer function for every sample. The equalizer is designed as a fractionally spaced equalizer (**FSE**) with 2 samples per symbol

(2 SpS), improving robustness against timing jitter and inter-symbol interference (ISI).In the built system the adaptive equalizer is a 2x2x10(**NTaps=10**) FIR filter with a convergence factor $\mu = [10^{-3}, 10^{-4}]$, using the greater for the first 12000 samples and then reduced to 10^{-4} to conserve the convergence.

In a nutshell:

1. $y[k] = w \cdot x$ (x is the input signal)

2. $e[k] = |y[k]|^2 - R$
   (R is the average power of the ideal constellation, $e[k]$ is computed only on even samples)

3. $w[k+1] = w[k] - \mu \cdot x \cdot e[k]y[k]$ (w weight matrix updated every sample)

Resampler

At the input of the resampler, the signal is still transmitted at 2 SpS. This block simply downsamples the signal in order to have 1 SpS. To select the optimal time instant, the two possible downsampled output signals are analyzed through their constellations (Figure 2.7).

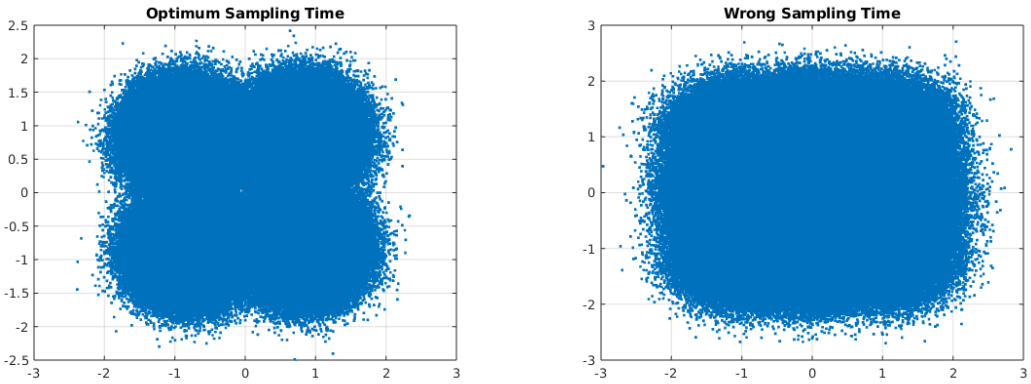

Figure 2.7: Downsampled Signal with SNR = 8 dB

From the figures above, it is very clear which is the correct downsampled signal, since it preserves the QPSK/DQPSK constellation shape.

Frequency Offset Compensation

Here, the signal (1 SpS) is passed through three equivalent algorithms, in order to estimate the frequency offset of the transmitter laser and then compensated.

$$y_{comp} = y \cdot e^{-j2\pi f_{est}}$$

The details of each algorithm will be examined later (Chapter 4).

Polarization Frame Alignment

The following block is needed for two main reasons. First of all, in the optical system the birefringence effect is considered, through a multiplication of the signal by a random unitary matrix. Furthermore, the used equalizer is of blind type, so it manages to separate perfectly the two polarizations, but swapping polarizations can happen as side effect of the equalization. This has to be properly handled, in order to have the transmitted and received signals perfectly aligned. Through a **likelihood** algorithm, computing the cross-correlation between the transmitted and received samples, any swap is detected, and then the transmitted signal will be aligned to the received one.

Carrier Phase Estimation

In a realistic scenario, DFB lasers emit light, whose power spectrum is not a delta pulse, but it has a "width" called linewidth ($\Delta\nu$) that can vary from a few kHz to 10 MHz. The laser phase noise considered in the research is directly proportional to the laser linewidth and has a **Lorentzian** spectrum [11]. In particular, the DFB lasers used in the PON context have linewidths in the order of unities of MHz. So, before decoding the signal, one last estimation has to be done: the **carrier phase estimation** (CPE). The implemented algorithm is based on the Viterbi-Viterbi algorithm and it uses pilots depending on the chosen modulation [7]. Besides, in the Figure 2.6, the block outline is dashed because, in Chapter 3, it will be discovered that with differential encoding, this step is not necessary. Finally, the CPE algorithm will be discussed in details in Chapter 3.

Decoder

At the end of the electrical dsp receiver, **Decoder** block is placed. The applied decoding technique is of the type hard decision (**HD**). So, setting as threshold 0, the received samples are forced to assume the following values: **1+1j**, **1-1j**, **-1+1j**, **-1-1j**. They are the ideal QPSK constellation points (see Figure 2.1). So, in conclusion, these samples can be demodulated using the same map mentioned in the subsection 2.1.1. Regarding the differential modulated signal, one further

step must be adopted before using the previously mentioned approach. In fact, reminding that the differential modulation encodes the **phase differences** between successive samples, at the decoder side, the phase difference must be recovered. In order to do that, it is simply requested to compute a multiplication between the received samples vector and the delayed and conjugated version of the same vector. After a normalization step, the signal results encoded as a QPSK and thus can be demodulated following the same steps described at the beginning of the paragraph.

Chapter 3

System Impact of Laser Phase Noise

3.1 Definition

For lasers used in communications field, linewidth can assume different values ($\Delta\nu_{DFB} = 1 \rightarrow 10\,\text{MHz}$) [12]. This is related to fluctuations of the optical phase of the laser output. Indeed, the laser will not exhibit a perfect sinusoidal oscillation of the electric field at its output. Consequently, there will be a kind of noise to take into account in the optical system: **laser phase noise**.
So, the transmitted signal will be affected by a random phase rotation:

$$x_{TX}[n] = x[n] \cdot e^{j\theta[n]}$$

where:

- x[n] is the nth sample of the ideal transmitted signal
- $\theta[n] = \theta[n-1] + \nu_n$
- ν_n is a Gaussian random variable with $\mu = 0$ and $\sigma^2 = 2\pi\frac{\Delta\nu}{Bw_{sim}}$

If we analyze the expression of the second point, it is a cumulative sum of normal distributions. In particular, it is said that the phase follows a random walk with small increments of Gaussian-type. Overall, this is named Wiener process, and its Fourier transform is the **Lorentzian** distribution. So, the power spectral density (**psd**) will have a shape very similar to a Gaussian, and the width of the Lorentzian peak will be correlated to the laser linewidth.

3.2 Carrier Phase Estimation Algorithm

In order to reduce penalty correlated to the phase noise the carrier phase of the signal has to be estimated and then compensated. The implemented algorithm follows the Viterbi-Viterbi phase estimation algorithm[7][10], and it can be summarized with the following fundamental steps:

1. $y_{RX}[n] = (a[n] + w[n]) \cdot e^{j\theta[n]}$

   where $a[n] = \sqrt{2}e^{j\pi/4}e^{jk\pi/2}$ is the modulated QPSK signal without noise (k = 1,2,3,4 which correspond to the 4 phase modulated bits).

2. $y_{RX}[n]^4 = 4e^{j\pi}e^{j2k\pi}e^{j4\theta[n]} + \bar{w}[n]$

3. $y_{RX}[n]^4 \approx -4e^{j4\theta[n]}$ where $\bar{w}[n]$ is averaged out with a moving average filter.

4. $\mathrm{sgn}(y_{RX}[n]^4) = \frac{y_{RX}[n]^4}{|y_{RX}[n]^4|} = T = -e^{j4\theta[n]}$

5. $\theta[n] = \frac{\angle T}{4}$

At point 2 the fourth-order (m = 4) power is evaluated to remove the QPSK/DQPSK modulation in order to have an unbiased estimator.

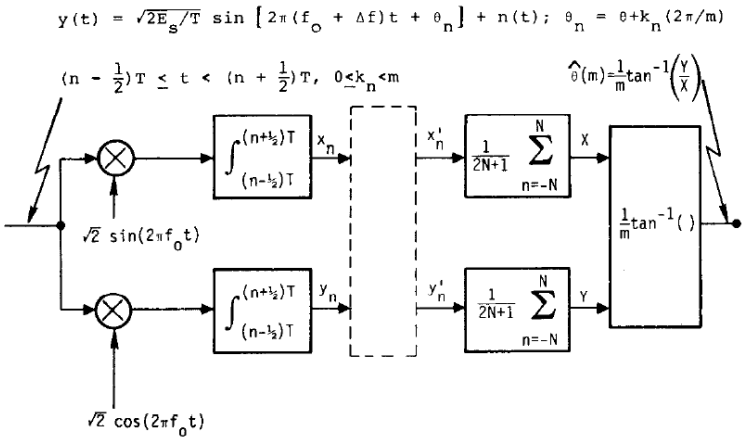

Figure 3.1: Basic phase estimator for m-PSK carriers [7]

"Obviously, if the carrier is phase modulated to one of m discrete phases, the above linear estimator is useless since during each successive symbol the phase takes on a different value"[7]. The m-power operation is executed into the dashed box which transforms $x_n, y_n \rightarrow x'_n, y'_n$.

3.3 Results

In the simulation part, in Section 3.3.1 and Section 3.3.2, it is shown the effect of phase noise on the system using QPSK and DQPSK, independently, looking at how the BER (Bit Error Rate) vs SNR (Signal to Noise Ratio) simulation curve differs from the analytic one.
In Section 3.3.3 the QPSK and DQPSK simulations are compared each other.

3.3.1 Comparison with Analytic Curve (QPSK)

First of all, some fundamental simulation parameters are listed in Table 3.1.

Parameter	**QPSK**
N_s (Symbols)	10^6
R_s (GBaud)	25
CPE	$N_{CPE} = 50$ samples
Pilots (Block Size)	$Bs_{CPE} = 32$ samples
Laser and LO Linewidth ($\Delta\nu$)	[1, 4] MHz

Table 3.1: QPSK simulation parameters with only **phase noise**

where:

- N_{CPE} is the Length of the moving average filter in CPE
- Bs_{CPE} is the separation (in terms of samples) between each phase pilot

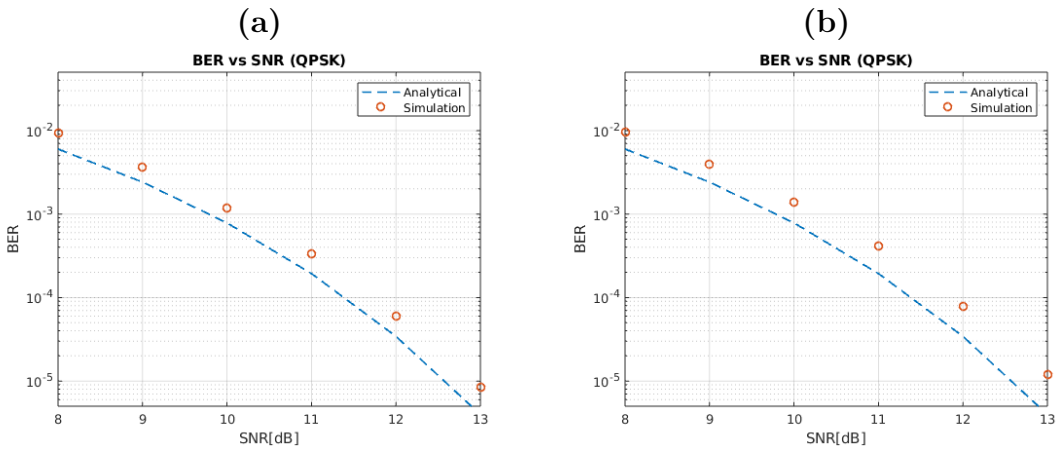

Figure 3.2: BER vs SNR Diagrams (QPSK)[**(a)**: $\Delta\nu = 1\,\text{MHz}$, **(b)**: $\Delta\nu = 2\,\text{MHz}$]

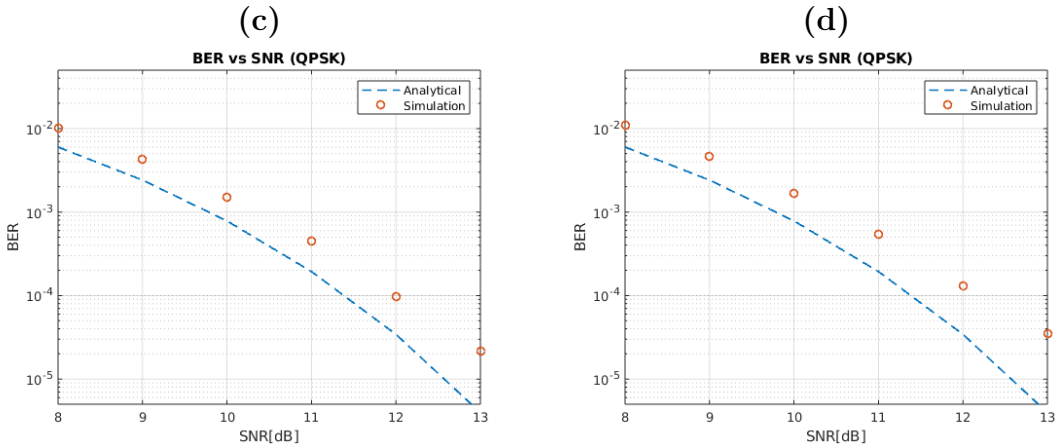

Figure 3.3: BER vs SNR Diagrams (QPSK)[**(c)**: $\Delta\nu = 3\,\text{MHz}$, **(d)**: $\Delta\nu = 4\,\text{MHz}$]

Looking closely at the simulated points, it can be clearly observed that, at increased linewidth ($\Delta\nu$), the distance between the simulation curve and the analytic one also increases. Technically, this is called **SNR penalty**, and is measured in dB. Furthermore, it means that to have a minimum certain level of BER, signal needs a higher SNR value, so consequently a greater received optical power. Finally, with a linewidth $\Delta\nu = 1$ MHz the penalty, for all SNR levels, is still negligible, but for $\Delta\nu \geq 2$ MHz the penalty starts to be considerable. **To be highlighted that these values of BER are evaluated before HD-FEC(Hard-Decision Forward Error Correction) codes.** They usually work

in a range of BER = $[10^{-3}; 10^{-2}]$. That is why, in the penalty analysis, the focus was more on these two thresholds (see Figure 3.4).

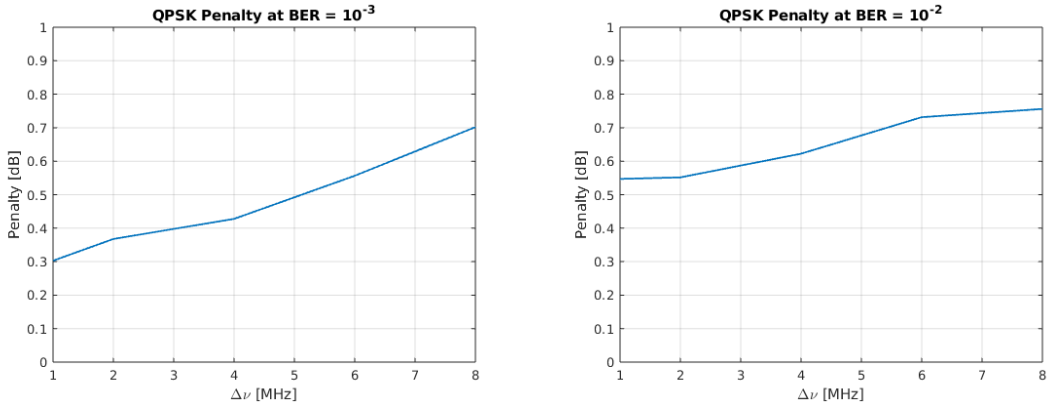

Figure 3.4: QPSK penalties vs $\Delta\nu$ at BER = $[10^{-3}; 10^{-2}]$

Here, it is more clear the direct proportionality between linewidth and penalty. First of all, a disclaimer must be done: **$\Delta\nu$ ticks in Figure 3.4 correspond to the sum of the linewidths of the laser and of the local oscillator** (i.e. $\Delta\nu = 1$ MHz$\rightarrow$ $\Delta\nu_{LAS} = 0.5$ MHz, $\Delta\nu_{LO} = 0.5$ MHz). Regarding BER = 10^{-3}, at $\Delta\nu = 1$ MHz we have a penalty slightly greater than 0.3 dB, negligible, but it grows almost linearly until 0.7 dB at 8 MHz, which means, in linear terms, that we need a power factor of 1.18 with respect to the ideal case, where we do not have phase noise. In BER = 10^{-2} case, at $\Delta\nu = 1$ MHz the penalty is already greater than 0.55 dB, not negligible, and reaches 0.75 dB at 8 MHz, corresponding to 1.19 in linear scale.

3.3.2 Comparison with Analytic Curve (DQPSK)

First of all, some fundamental simulation parameters are listed in Table 3.2.

Parameter	**DQPSK**
N_s (Symbols)	10^6
R_s (GBaud)	25
CPE	**NO CPE**
Pilots (Block Size)	**NO PILOTS**
Laser and LO Linewidth ($\Delta\nu$)	[1, 4] MHz

Table 3.2: DQPSK simulation parameters with only **phase noise**

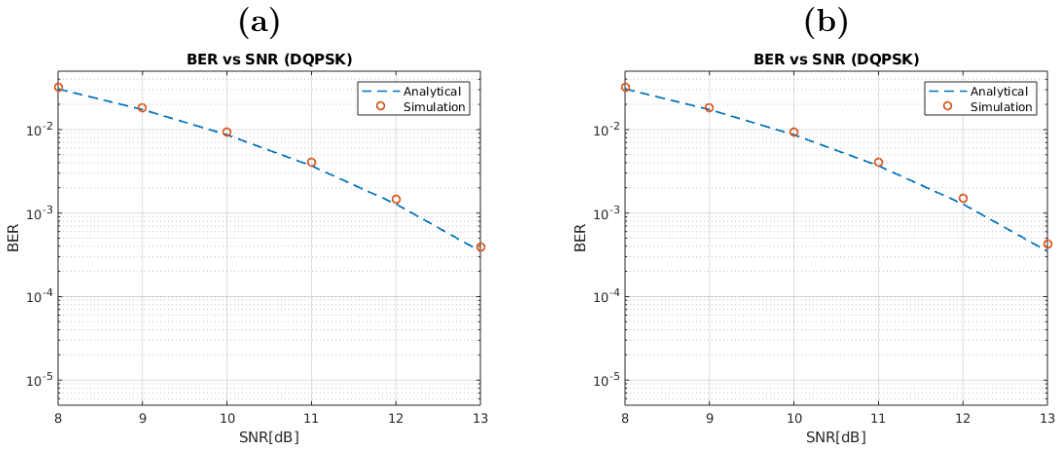

Figure 3.5: BER vs SNR Diagrams (DQPSK)[**(a)**:$\Delta\nu = 1\,\text{MHz}$, **(b)**:$\Delta\nu = 2\,\text{MHz}$]

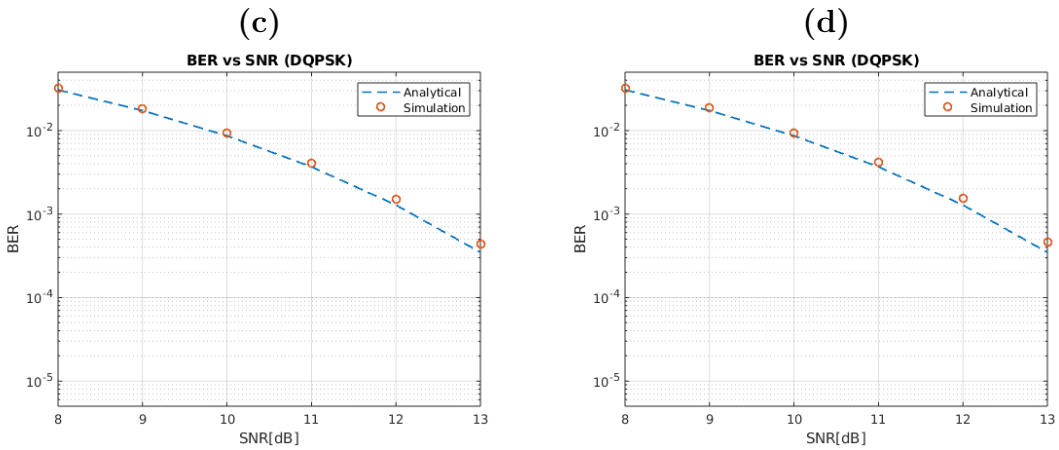

Figure 3.6: BER vs SNR Diagrams (DQPSK)[**(c)**:$\Delta\nu = 3\,\text{MHz}$, **(d)**:$\Delta\nu = 4\,\text{MHz}$]

Differently from QPSK case, the simulation and the analytical curves almost match. In fact, it seems the simulated points lie on the analytical curve. So, the first obtained result is **DQPSK does not suffer from this laser phase noise**. Also, DQPSK is not affected by any quantity of phase noise. At a glance, the four above figures (Figure 3.5, Figure 3.6) look identical each other. In other words, the penalty with respect to the analytical curve, changing linewidths, is very small, negligible and even more important seems constant. To confirm these first results, the same penalty analysis of Section 3.3.1 is performed. Even in this case, two BER thresholds are analyzed: BER = $[10^{-3}; 10^{-2}]$ [1].

[1] **these values of BER are evaluated before FEC (Forward Error Correction) codes.** They usually work in a range of BER = $[10^{-3}; 10^{-2}]$. That is why, in the penalty analysis, the focus was on these two specific thresholds.

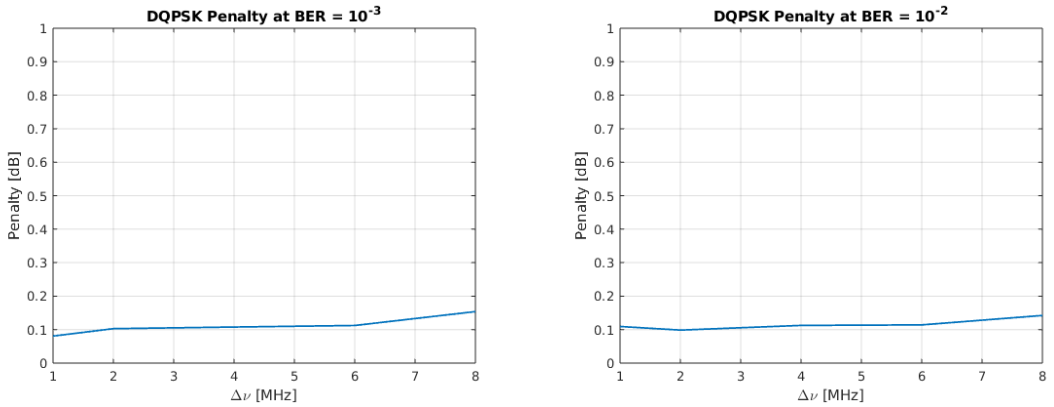

Figure 3.7: DQPSK penalties vs $\Delta\nu$ at BER = $[10^{-3}; 10^{-2}]$

Looking [2] at Figure 3.7, we can see that the penalty is not perfectly constant, but it grows linearly with the linewidth, but with a really small slope. With BER = 10^{-3}, at $\Delta\nu = 1$ MHz the corresponding penalty is slightly lower than 0.1 dB, while at $\Delta\nu = 8$ MHz the penalty is 0.15 dB circa. A very similar result is obtained when the penalty is estimated for BER = 10^{-2}. Even though the final behavior of the penalty with respect to linewidth is not perfectly constant in both figures, it can be safe to approximate these lines to horizontal lines, and consequently claim and confirm that:**"Laser phase noise has a negligible penalty on DQPSK"**. Also, looking carefully at the list of parameters at the beginning of Section 3.3.2, another significant difference, with respect to the previous QPSK case, is the **total absence of CPE block** in the DSP receiver chain. This means that **the shown results are obtained with a fully blind DSP receiver**, from the equalizer to the decoder. The removed CPE block translates to reduced run time for symbols transmission and lower hardware cost and complexity. Furthermore, not using pilots there is not waste of symbols into the packets' payload.

[2] **$\Delta\nu$ ticks in Figure 3.7 correspond to the sum of the linewidths of the laser and of the local oscillator** (i.e. $\Delta\nu = 1$ MHz$\rightarrow$ $\Delta\nu_{LAS} = 0.5$ MHz, $\Delta\nu_{LO} = 0.5$ MHz).

3.3.3 Discussion and Comparison

In this paragraph, DQPSK and QPSK simulations are directly compared. The used DSP receivers are slightly different, given, above all, the CPE block removal. As a reminder, the main parameters are shown for both versions:

Parameter	**QPSK**	**DQPSK**
N_s (Symbols)	10^6	10^6
R_s (GBaud)	25	25
CPE	$N_{CPE} = 50$ samples	**NO CPE**
Pilots (Block Size)	$Bs_{CPE} = 32$ samples	**NO PILOTS**
Laser and LO Linewidth ($\Delta\nu$)	[1,4] MHz	[1,4] MHz

Table 3.3: Comparison of QPSK and DQPSK simulation parameters

The whole analysis is carried out in terms of **BER** (BER vs SNR diagram), and **required SNR** (req_snr vs $\Delta\nu$).

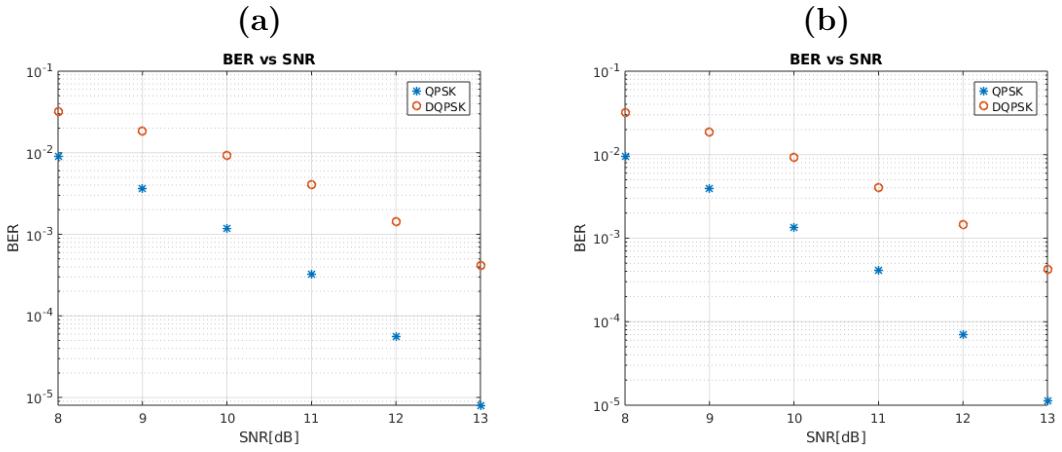

Figure 3.8: BER vs SNR Diagrams (QPSK vs DQPSK)[**(a)**:$\Delta\nu = 1$ MHz, **(b)**:$\Delta\nu = 2$ MHz]

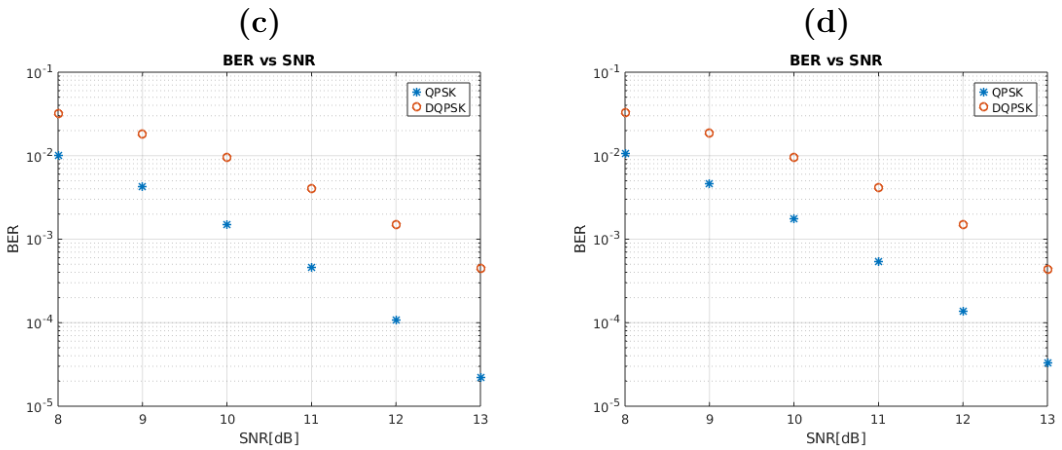

Figure 3.9: BER vs SNR(QPSK vs DQPSK)[**(c)**:$\Delta\nu = 3\,\text{MHz}$, **(d)**:$\Delta\nu = 4\,\text{MHz}$]

From Figure 3.8 and Figure 3.9, it is clear that QPSK obtains better BER results with respect to DQPSK. In fact, even increasing $\Delta\nu$ (increasing phase noise), the two curves are very distinguishable, with the DQPSK simulation points well above QPSK points. But it is evident the mismatch between the curves shrinks for growing linewidth. This is motivated by the results shown in section 3.3.1 and section 3.3.2, where it was demonstrated that QPSK is affected by phase noise, with overall increasing penalty with respect to ideal scenario ($\Delta\nu = 0$), while DQPSK behavior is approximately identical to the analyticak curve (0.1 dB penalty).
For a quantitative analysis of the discrepancy between QPSK and DQPSK, the **required SNR** is estimated. In particular, this quantity is used for power budget estimation, since, to maintain a certain BER, the system must ensure sufficient received optical power, especially in the presence of noise and channel impairments.

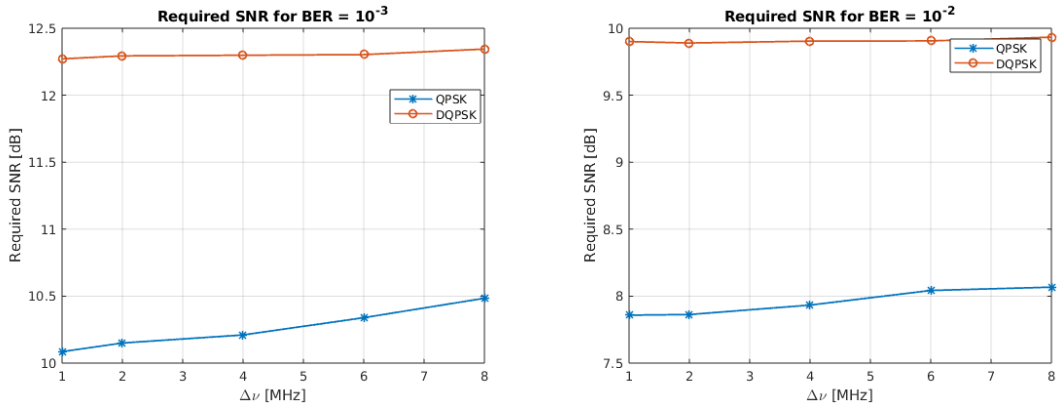

Figure 3.10: Required SNR vs $\Delta\nu$ for BER = $[10^{-3}; 10^{-2}]$

In Figure 3.10, [3] it can be noticed QPSK requires higher SNR for greater $\Delta\nu$, while DQPSK can guarantee the BER level for any quantity of phase noise, not asking additional SNR. In particular, to ensure BER = 10^{-3}, QPSK needs 10.1 dB of SNR at 1 MHz of linewidth, and 10.5 dB SNR circa at $\Delta\nu = 8$ MHz. Regarding DQPSK, the required SNR is almost constant, around 12.3 dB, so the displacement between QPSK and DQPSK goes from 2.2 dB ($\Delta\nu = 1$ MHz) to 1.8 dB ($\Delta\nu = 8$ MHz). Same comments can be referred to required SNR for BER = 10^{-2}, where the discrepancy between the curves ranges between 2 and 1.8 dB.
As a final statement it can be fair to claim that QPSK presented better results in terms of BER and required SNR with respect to DQPSK. On the other hand, instead it is fundamental to highlight the conditions under which they work. QPSK needs a Data-Aided (DA) Carrier Phase Estimation (CPE) stage to reduce the impact of cycle slip events. DQPSK has no constraints in terms of CPE, pilots and above all, amount of phase noise that can tolerate, making it more robust than QPSK. Consequently, this kind of modulation can be used in any real scenario, so very useful for heterogeneous working conditions as in the PON context.

[3] **$\Delta\nu$ ticks in Figure 3.10 correspond to the sum of the linewidths of the laser and of the local oscillator** (i.e. $\Delta\nu = 1$ MHz$\rightarrow$ $\Delta\nu_{LAS} = 0.5$ MHz, $\Delta\nu_{LO} = 0.5$ MHz).

Chapter 4

System Impact of Frequency Offset

4.1 Definition

In Passive Optical Network (PON) scenarios, Distributed Feedback (DFB) lasers are commonly used as optical transmitters due to their cost-effectiveness. However, these lasers are susceptible to frequency offset, which refers to a deviation from the nominal laser frequency (f_c).
This offset arises due to manufacturing variations, temperature fluctuations, and aging effects, leading to instability in the transmitted optical signal.
A significant frequency offset can cause serious issues in coherent detection systems, including **impaired carrier recovery, reduced signal-to-noise ratio (SNR), and increased phase noise**. In extreme cases, it may lead to interchannel interference in dense wavelength-division multiplexing (DWDM) systems, degrading overall network performance. Furthermore, frequency offset impacts the effectiveness of digital signal processing (DSP) algorithms, which are crucial for compensating chromatic dispersion and phase noise in coherent receivers. Now, a few modifications have to be applied, in order to consider frequency offset into the transmitted signal. They can be summed up to the following expression:

$$x_{TX}[n] = x[n] \cdot e^{j\theta[n]} \cdot e^{2\pi \Delta f \, n \, T_s}$$

- $e^{j\theta[n]}$ is the phase noise (see Chapter 3)
- Δf is the frequency offset
- T_s is the sampling period

4.2 Frequency Offset Compensation Algorithms

In PON environments, where cost constraints limit the complexity of transceivers, managing frequency offset becomes particularly challenging. This makes it essential to design robust DSP techniques and adaptive compensation methods to ensure reliable communication even under significant frequency offset conditions.
The three algorithms, described in the following sections for Frequency Offset Compensation (**FOC**), estimate different frequency ranges using a non data aided approach (NDA).

4.2.1 Differential Phase-Based Method

The first algorithm is based on a non data-aided feed forward approach. The goal is to estimate the phase shift between two consecutive samples (differential) that is caused by a frequency offset Δf between transmitter and LO laser, as indicated in Figure 4.1.

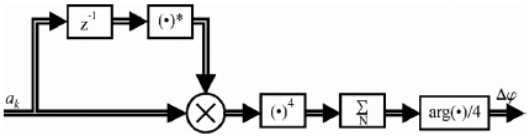

Figure 4.1: Block diagram of the frequency estimator

Then, inverting the formula $\Delta\phi = 2\pi\Delta f\, T_s$ [13], the frequency offset can be estimated. The overall formula is [10]:

$$\Delta f = \frac{1}{8\pi\, T_{sym}} \arg\{\sum_{k=1}^{N} (x_{in}[k] x_{in}^*[k-1])^4\} \quad \text{with } \Delta f_{max} = \frac{R_s}{16} \approx 1.56\,\text{GHz}$$

Alternatively, there is also an iterative version in [10]-[14], but not implemented here.

4.2.2 Spectral Method

The following algorithm is implemented by observing the peak in the spectrum of x_{in}^4 [10]:

$$\Delta f = \arg\, \max_{\Delta f} \sum_{K=1}^{N} x_{in}^4[k]\, e^{-8j\pi k \Delta f T_{sym}} \quad \text{with } \Delta f_{max} = \frac{R_s}{8} \approx 3.12\,\text{GHz}$$

From another point of view, this can be seen as a Maximum Likelihood (ML) estimation of the argument of demodulated signal (x_{in}^4). In a range ([-3 GHz, 3

GHz] with resolution 1 MHz) of frequencies, it is chosen the one that maximizes the ML.

4.2.3 FFT-Based Method

In the last algorithm, it is not needed to remove the modulation, but it is observed the frequency peak (f_{peak}) of the FFT of the angle ($\angle x_{in}$). Starting from [15], it is simply demonstrated that $|\Delta f_1| = \frac{f_{peak}}{4}$ and compensation is applied, ignoring the sign. Then, the algorithm is repeated and $|\Delta f_2|$ is estimated.
Finally, $\Delta f_1 = \text{sign}\{|\Delta f_1| - |\Delta f_2|\}|\Delta f_1|$, and the correct compensation can be applied to x_{in} (see Figure 4.2).

$$x = x_{in} \cdot e^{-j2\pi\Delta f_1}$$

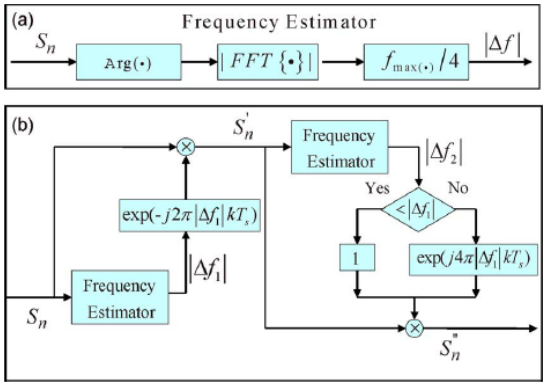

Figure 4.2: Block diagram of the algorithm. (a)Frequency estimator by employing FFT; (b) the whole structure of the algorithm [15].

Because of sign ambiguity, estimation range is not symmetric ($\Delta f = [-\frac{R_s}{12}, \frac{R_s}{8}]$). To enhance it, in [16], an improved version is proposed. With respect to before, just a couple of steps are added. A frequency threshold is set according to the following condition:

$$|\Delta f|_{th} = \begin{cases} |\Delta f_1|, & |\Delta f_1| \leq \frac{R_s}{16} \\ \frac{R_s}{8} - |\Delta f_1|, & |\Delta f_1| > \frac{R_s}{16} \end{cases}$$

As last step, $\Delta f = \text{sign}\{|\Delta f|_{th} - |\Delta f_2|\}|\Delta f_1|$.

From now on, the estimation range will be $\Delta f = [-\frac{R_s}{8}, \frac{R_s}{8}]$.

4.3 Results

After the addition of frequency offset phenomenon, the DSP receiver framework is therefore modified in order to properly estimate and compensate for the frequency offset between transmitter laser and local oscillator (**FOC**).

First of all (Section 4.3.1), the implemented FOC algorithms are analyzed, to find the most adapt to metro/access optical networks scenarios.

In Section 4.3.2 and Section 4.3.3, each simulation is compared with its corresponding analytic BER vs SNR curve to estimate the penalty behavior at the frequency offset and laser phase noise variations.

In Section 4.3.4, realistic access/metro networks conditions will be considered. The system will be tested under **high phase noise** ($\Delta\nu = [2,4]$ MHz) and **huge frequency offset** ($\Delta f = [1,3]$ GHz). Here, the two modulation formats are directly compared analyzing their performances in terms of BER vs SNR diagrams and Required SNR.

In Section 4.3.5, a final comparison between QPSK and DQPSK simulations is executed, estimating the overall time needed to the whole system to converge (**preamble duration**).

4.3.1 FOC Algorithms Comparison

The introduction of frequency offset between laser and local oscillator brings to consider a compensation stage, otherwise huge penalties would arise, causing high BER, degrading severely transmission performances. During the research phase, three algorithms have been implemented: **Differential Phase-Based Method**, **Spectral Method** and **FFT-Based Method**. Full details can be found in Section 4.2.1, Section 4.2.2, Section 4.2.3.
Here, they will be compared in terms of **convergence time**, **robustness to phase noise** and **run time**.
The first tests were executed under low phase noise conditions ($\Delta\nu = 500\,\text{kHz}$) and different frequency offset values (1, 2, 3 GHz), giving already some hints to which could be the best algorithm to use in PON scenarios. Both modulations (QPSK (**blue**) and DQPSK (**red**)) were tested. For the sake of clarity, only the worst case scenario ($\Delta f = 3\,\text{GHz}$) results are shown.
As discussed before (Section 4.2.1), Differential Phase-Based method can not be used with $|\Delta f| > 1.5\,\text{GHz}$. Looking at Figure 4.3, the curve converges steadily only after ~ 15000 samples.

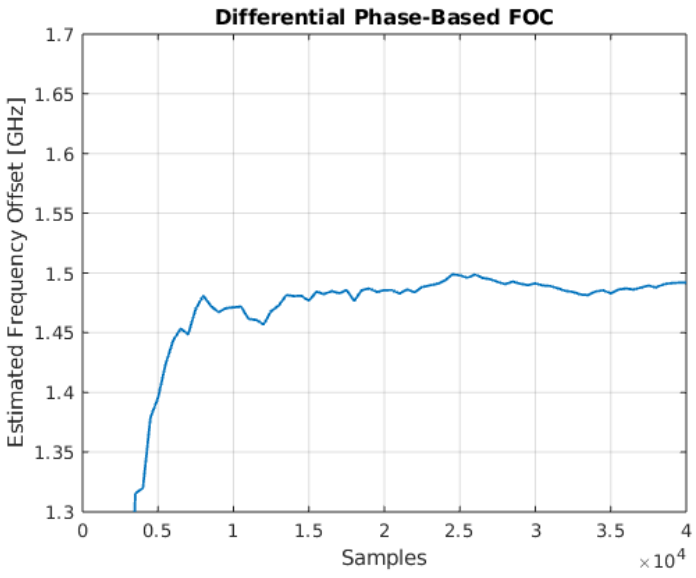

Figure 4.3: Differential Phase-Based Method convergence time(QPSK) [$\Delta\nu = 500\,\text{KHz}$, $\Delta f = 1.5\,\text{GHz}$]

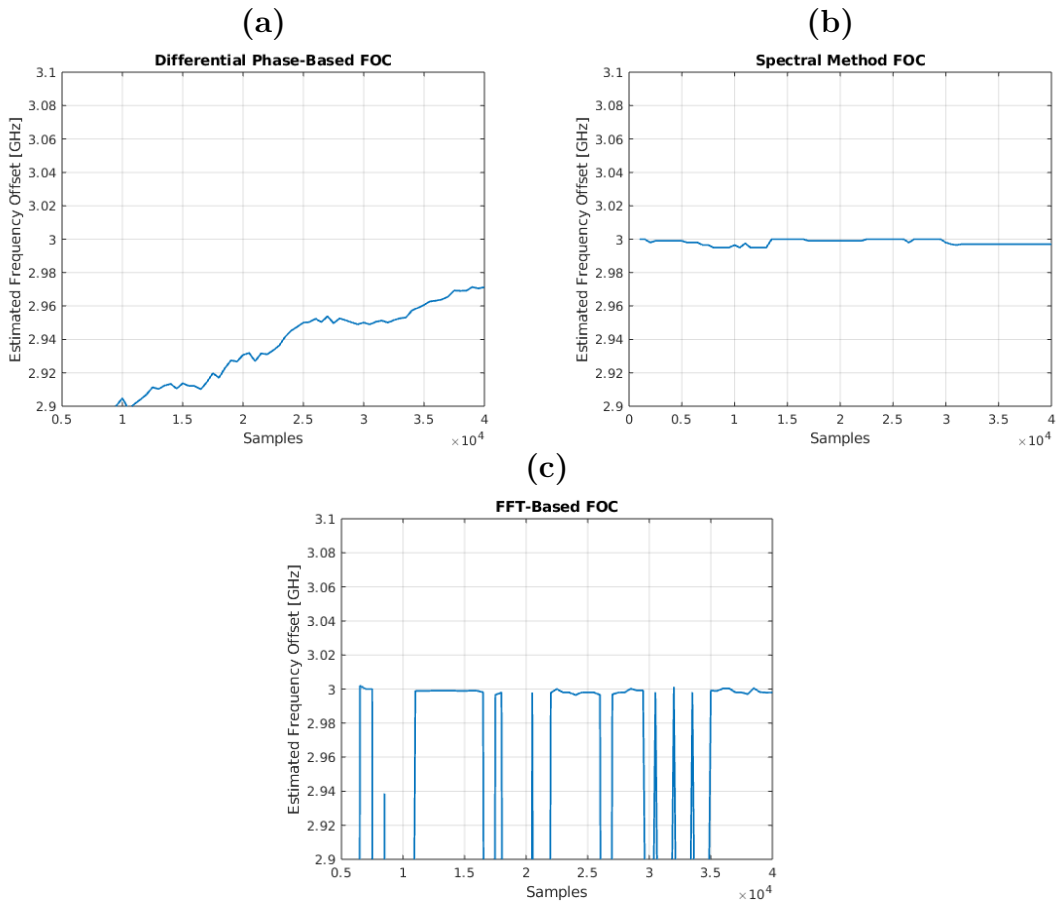

Figure 4.4: FOC Convergence Times (QPSK)
(a):$\Delta\nu = 500\,\text{kHz},\ \Delta f = 3\,\text{GHz}$
(b):$\Delta\nu = 500\,\text{kHz},\ \Delta f = 3\,\text{GHz}$
(c):$\Delta\nu = 500\,\text{kHz},\ \Delta f = 3\,\text{GHz}$

The spectral method (Figure 4.4(b)) is clearly the best among the three algorithms. It converges almost instantaneously, with some little riddle at the beginning. FFT-Based (Figure 4.4(c)) is very accurate, but at the same time very unstable since it oscillates a lot, and it does not really completely converge. So, even though, theoretically, FFT-Based algorithm is able to estimate $|\Delta f| \leq 3\,\text{GHz}$, the presence of phase noise affects severely its estimation range. Regarding the differential one, it can be considered a reliable algorithm for $\Delta f \leq 1.5\,\text{GHz}$ (Figure 4.3), but not accurate enough for $\Delta f > 1.5\,\text{GHz}$ (Figure 4.4(a)), since it only reaches 2.97 GHz (after 40000 samples), corresponding to an estimation error of $\sim$ 30 MHz (not negligible).

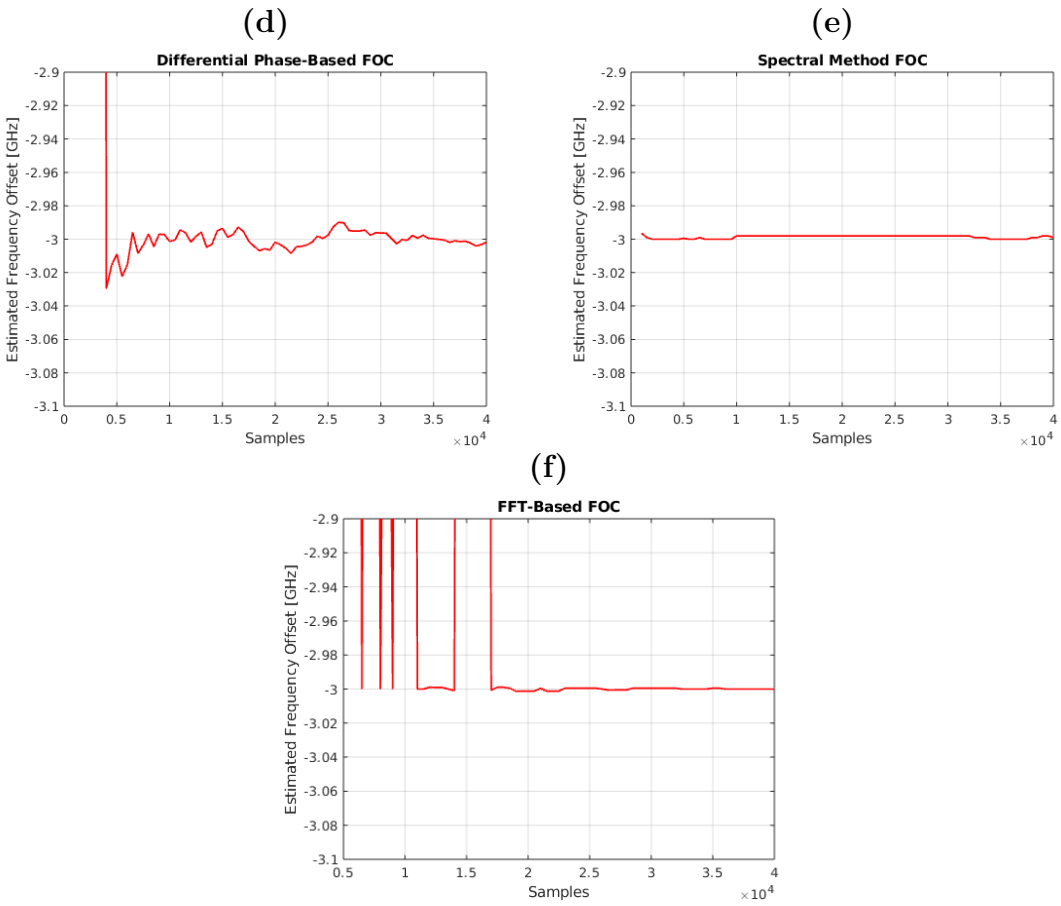

Figure 4.5: FOC Convergence Times (DQPSK)
(d):$\Delta\nu = 500\,\text{kHz},\ \Delta f = 3\,\text{GHz}$
(e):$\Delta\nu = 500\,\text{kHz},\ \Delta f = 3\,\text{GHz}$
(f):$\Delta\nu = 500\,\text{kHz},\ \Delta f = 3\,\text{GHz}$

With DQPSK, the results are much more promising with respect to QPSK. Surprisingly, either of the three FOC algorithms converges. The differential one (Figure 4.5(d)) needs at least 7000 samples to have an acceptable estimate, even though it continues to slightly oscillate. For FFT-Based FOC (Figure 4.5(f)), the system fully stabilizes, with great accuracy, after 17000 samples ca.. Finally, regarding Spectral Method (Figure 4.5(e)), same performances as in QPSK case are found, with convergence only after 2000 samples and a perfect stability. So, using a DQPSK system, each of the three algorithms could be interchangeably used.
Even if $\Delta f = 3\,\text{GHz}$, in DQPSK case, the estimated $\Delta f_{est} = -3\,\text{GHz}$. However, the result of the BER curve is correct, which means that the algorithm works perfectly. In fact, looking at the power spectrum of the signal at the input of the

equalizer, it is centered at 3 GHz, but after the equalization, the signal power spectrum is centered at -3 GHz, so the fully blind equalizer flips the signal (Figure 4.7). However, this phenomenon does not occur with the QPSK modulation format (Figure 4.6).

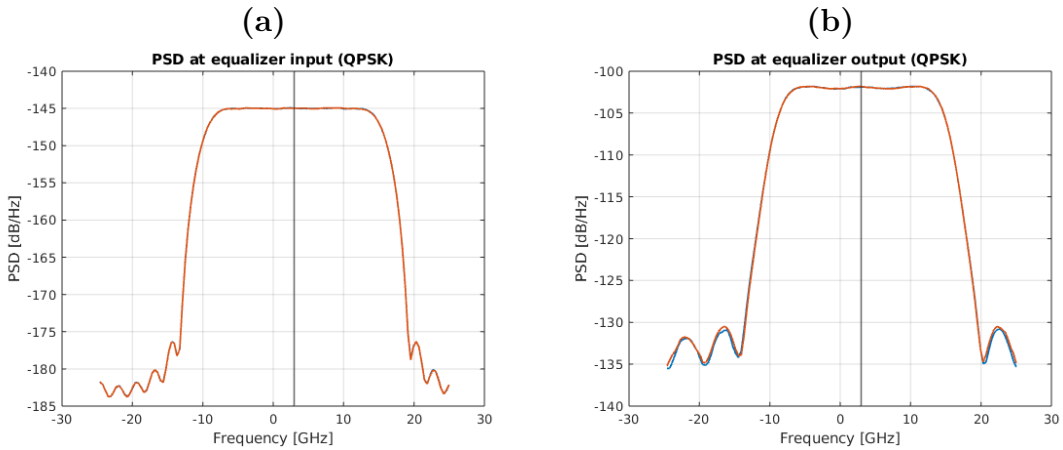

Figure 4.6: Power Spectral Density (PSD) of QPSK signal
(a): at equalizer input
(b): at equalizer output

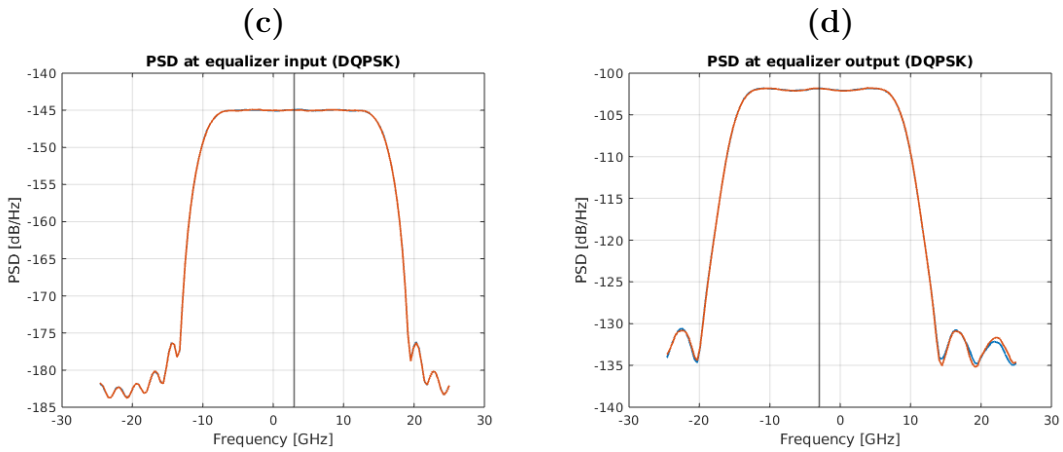

Figure 4.7: Power Spectral Density (PSD) of DQPSK signal
(c): at equalizer input
(d): at equalizer output

As a final test, the only two algorithms, both suitable with QPSK and DQPSK, were checked under a huge load of phase noise ($\Delta\nu = 4\,\text{MHz}$)[1].

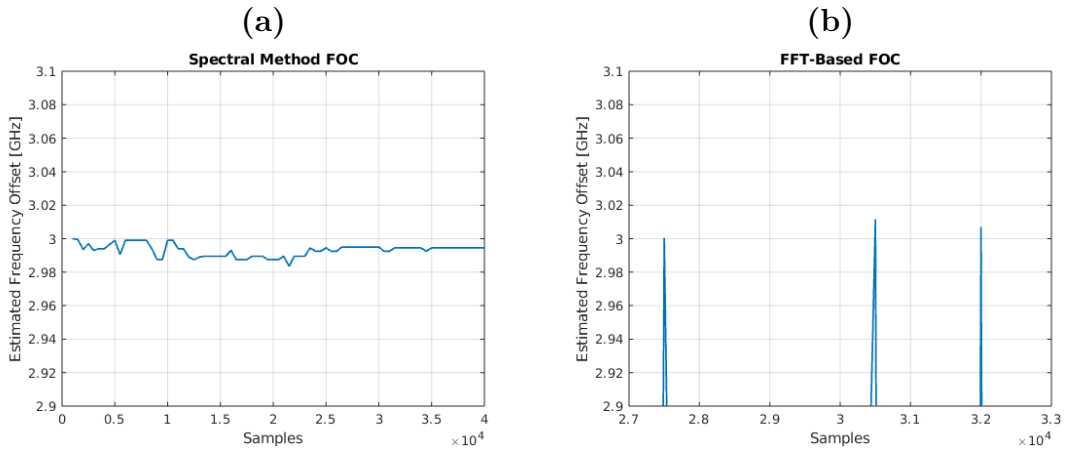

Figure 4.8: FOC Convergence Times (QPSK)
(a):$\Delta\nu = 4\,\text{MHz}$, $\Delta f = 3\,\text{GHz}$
(b):$\Delta\nu = 4\,\text{MHz}$, $\Delta f = 3\,\text{GHz}$

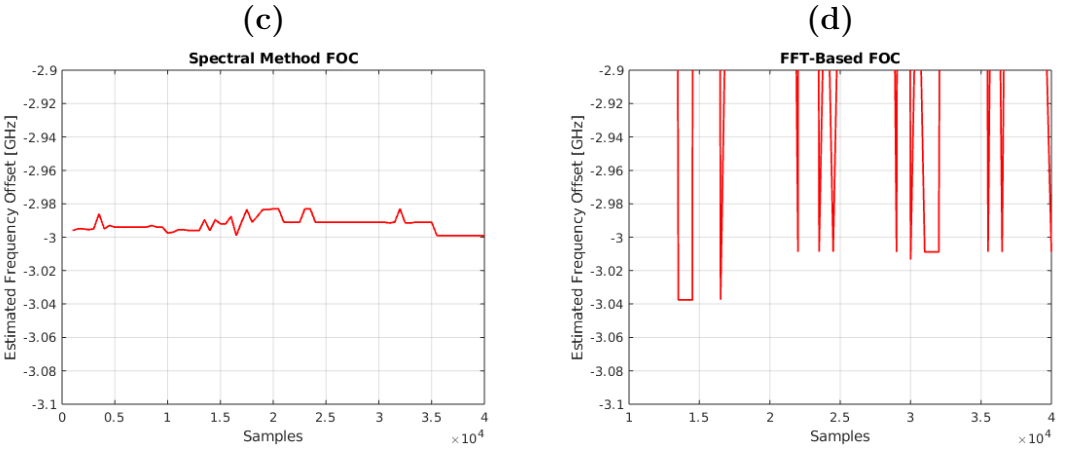

Figure 4.9: FOC Convergence Times (DQPSK)
(c):$\Delta\nu = 4\,\text{MHz}$, $\Delta f = 3\,\text{GHz}$
(d):$\Delta\nu = 4\,\text{MHz}$, $\Delta f = 3\,\text{GHz}$

[1]In this case $\Delta\nu = 4\,\text{MHz}$ means that both the transmitter laser and local oscillator have a linewidth of 4 MHz)

From Figure 4.8 and Figure 4.9, it is evident that under certain conditions of high phase noise and high frequency offset, the only choice for FOC is the **Spectral-Based method**, much more robust, stable and accurate with respect to the other two. Obviously, the other implemented FOC algorithms can still be applied in other contexts, where phase noise is not huge (FFT-based), or if the frequency offset is lower than $\frac{R_s}{16}$ (Differential Phase-Based)[2].

Context (QPSK)	**Diff-Phase**	**Spectral**	**FFT**
$\Delta\nu \leq 500\,\text{kHz}$ $\lvert\Delta f\rvert \leq \frac{R_s}{16}$	✓	✓	✓
$\Delta\nu \leq 500\,\text{kHz}$ $\frac{R_s}{16} \leq \lvert\Delta f\rvert \leq \frac{R_s}{8}$		✓	✓
$\Delta\nu \leq 4\,\text{MHz}$ $\lvert\Delta f\rvert \leq \frac{R_s}{8}$		✓	

Table 4.1: FOC Algorithms Comparison in different scenarios (QPSK)

Context (DQPSK)	**Diff-Phase**	**Spectral**	**FFT**
$\Delta\nu \leq 500\,\text{kHz}$ $\lvert\Delta f\rvert \leq \frac{R_s}{16}$	✓	✓	✓
$\Delta\nu \leq 500\,\text{kHz}$ $\frac{R_s}{16} \leq \lvert\Delta f\rvert \leq \frac{R_s}{8}$	✓	✓	✓
$\Delta\nu \leq 4\,\text{MHz}$ $\lvert\Delta f\rvert \leq \frac{R_s}{8}$		✓	

Table 4.2: FOC Algorithms Comparison in different scenarios (DQPSK)

[2] $\Delta\nu$ is the linewidth of each laser in the system (transmitter laser and local oscillator), Δf is the frequency offset between transmitter laser and local oscillator

One last comment relates to complexity. The three algorithms present three different levels of complexity. The most complex one is the spectral method. This aspect was studied in terms of run time (Table 4.3), using the same server, with the following technical specifics:

Server Technical Specifications

Processor: 4x Intel(R) Xeon(R) E5-4627 v2 @ 3.30GHz
Cores: 32 CPUs (4 sockets, 8 cores per socket)
RAM: 125GB
Operating System: Ubuntu 24.04 LTS

///	**Diff-Phase**	**Spectral**	**FFT**
Run Time [s]	0.0133	1.8521	0.0272

Table 4.3: FOC Algorithms Complexity

Obviously, to make a fair comparison, they are tested in **Context 1** of Table 4.1, Table 4.2, where either of them works perfectly.
It is quite clear the Differential Phase-Based is the fastest, while Spectral method is the slowest.
However, from now on, in the next shown results, the FOC algorithm implemented in the simulated DSP receiver is only the **Spectral Method**, because of its great accuracy and robustness in frequency estimation, although it is the slowest.

4.3.2 Comparison with Analytic Curve (QPSK)

First of all, some fundamental simulation parameters are listed:

Parameter	**QPSK**
N_s (Symbols)	10^6
R_s (GBaud)	25
CPE	$N_{CPE} = 50$ samples
Pilots (Block Size)	$Bs_{CPE} = 32$ samples
Laser and LO Linewidth ($\Delta\nu$)	[2; 4] MHz
Frequency Offset (Δf)	[1, 3] GHz
FOC Algorithm	**Spectral Method**

Table 4.4: QPSK simulation parameters with **phase noise** and **frequency offset**

In this context, frequency offset refers to the difference between the optical carrier frequency of the transmitter laser and that of the local oscillator in a coherent receiver. Also, even though in the shown results the chosen Δf are always positive, the same results can be achieved with negative frequency offsets, since the estimation range of the FOC algorithm is perfectly symmetrical. In Figure 4.10 and Figure 4.11, QPSK simulations are shown in terms of BER vs SNR diagrams, where linewidth is fixed($\Delta\nu = [2; 4]\,\text{MHz}$) and frequency offset is variable($\Delta f = 1 \rightarrow 3\,\text{GHz}$).

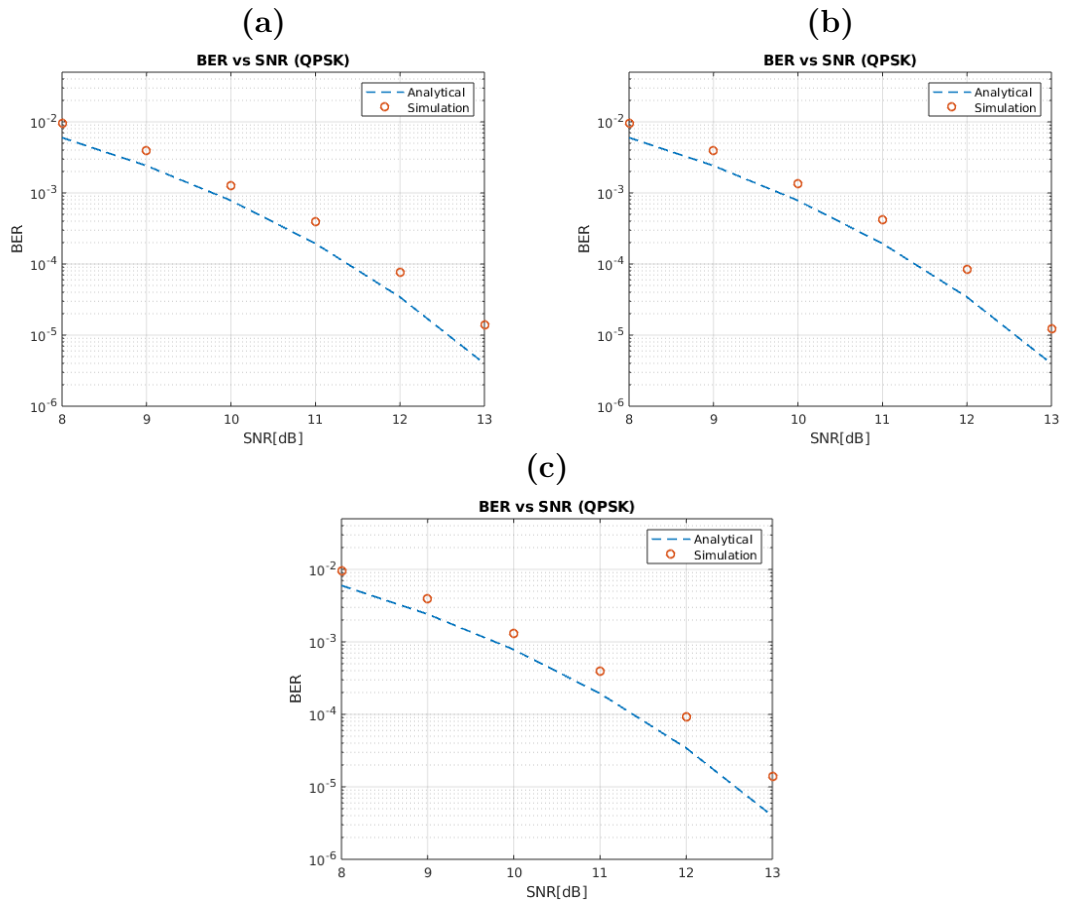

Figure 4.10: BER vs SNR Diagrams (QPSK)
(a):$\Delta\nu = 2\,\text{MHz},\ \Delta f = 1\,\text{GHz}$
(b):$\Delta\nu = 2\,\text{MHz},\ \Delta f = 2\,\text{GHz}$
(c):$\Delta\nu = 2\,\text{MHz},\ \Delta f = 3\,\text{GHz}$

According to the three figures above, if they are compared each other they seem very similar, so the FOC algorithm [3]estimates and compensates perfectly the frequency offset between laser and local oscillator. Also, at a glance, Figure 4.10 looks matching Figure 3.2(b), where only phase noise is present, so frequency offset does not add any further penalty.

[3]The Frequency Offset Compensation algorithm used for simulation is the Spectral Method (Section 4.2.2)

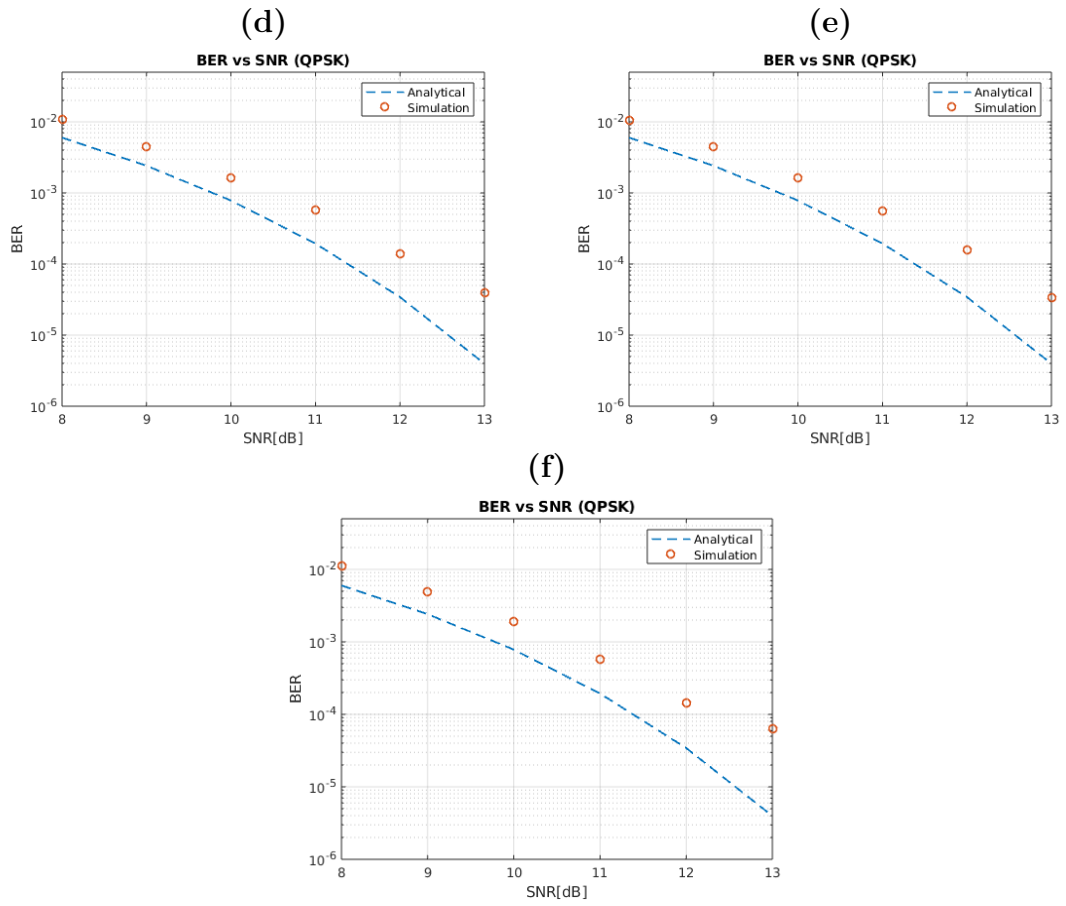

Figure 4.11: BER vs SNR Diagrams (QPSK)
(d):$\Delta\nu = 4\,\text{MHz},\ \Delta f = 1\,\text{GHz}$
(e):$\Delta\nu = 4\,\text{MHz},\ \Delta f = 2\,\text{GHz}$
(f):$\Delta\nu = 4\,\text{MHz},\ \Delta f = 3\,\text{GHz}$

Even in this case, where the linewith is increased to $\Delta\nu = 4\,\text{MHz}$, the simulated points do not apparently change their values for growing frequency offsets. And, again, as in previous case, Figure 4.11 looks equal to Figure 3.3(b), confirming the good performances of the implemented FOC algorithm[4]. In order to safely guarantee what was just said, a penalty analysis is carried out for either of the frequency offset cases ($\Delta f = 1\,\text{GHz}, 2\,\text{GHz}, 3\,\text{GHz}$).

[4]The Frequency Offset Compensation algorithm used for simulation is the Spectral Method (Section 4.2.2)

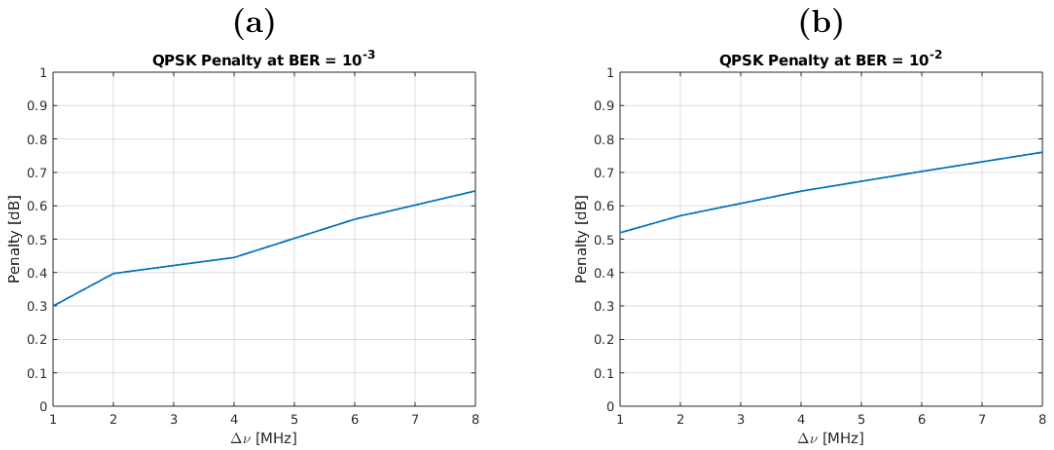

Figure 4.12: QPSK penalties vs $\Delta\nu$ at BER = $[10^{-3}; 10^{-2}]$ with $\Delta f = 1\,\mathrm{GHz}$

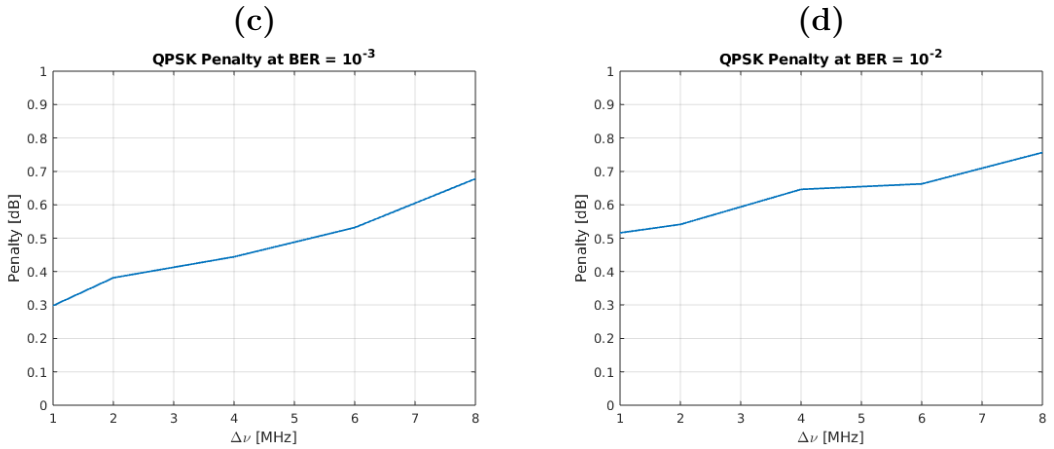

Figure 4.13: QPSK penalties vs $\Delta\nu$ at BER = $[10^{-3}; 10^{-2}]$ with $\Delta f = 2\,\mathrm{GHz}$

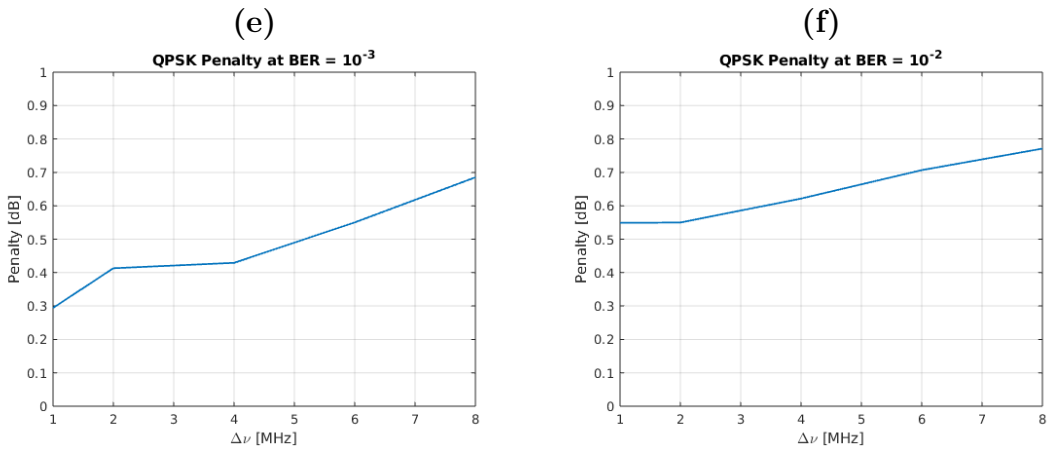

Figure 4.14: QPSK penalties vs $\Delta\nu$ at BER = $[10^{-3}; 10^{-2}]$ with $\Delta f = 3\,\text{GHz}$

Even though the plots, for each frequency offset value (Figure 4.12(a), 4.13(c), 4.14(e) or Figure 4.12(b), 4.13(d), 4.14(f)), are not perfectly identical, they can be considered perfectly equivalent[5]. In fact, with or without frequency offset, at BER=10^{-3} the penalty goes from $\sim$ 0.3 dB, at $\Delta\nu = 1\,\text{MHz}$, up to 0.65 dB, at $\Delta\nu = 8\,\text{MHz}$ [6].
At BER=10^{-2} the computed penalty ranges from around 0.5 dB, at $\Delta\nu = 1\,\text{MHz}$, up to 0.75 dB, at $\Delta\nu = 8\,\text{MHz}$.
Furthermore, if they are compared with the ones obtained without frequency offset (Figure 3.4), they can be considered equal.
Finally, it was verified what observed in the BER vs SNR diagrams, confirming that frequency offset does not impact QPSK performances overall. Obviously, this is valid only within the FOC algorithm estimation range[7], where it manages to estimate almost perfectly the frequency offset between the laser and the local oscillator.

[5] $\Delta\nu$ **ticks in Figure 4.12, Figure 4.13, Figure 4.14, correspond to the sum of the linewidths of the laser and of the local oscillator** (i.e. $\Delta\nu = 1$ MHz$\rightarrow$ $\Delta\nu_{LAS} = 0.5$ MHz, $\Delta\nu_{LO} = 0.5$ MHz).

[6] **These values of BER are evaluated before FEC (Forward Error Correction) codes.** They usually work in a range of BER = $[10^{-3}; 10^{-2}]$. That is why, in the penalty analysis, the focus was on these two specific thresholds.

[7] $\Delta f_{est} = [-\frac{R_s}{8}, \frac{R_s}{8}] \approx [-3, 3]\,\text{GHz}$

4.3.3 Comparison with Analytic Curve (DQPSK)

First of all, some fundamental simulation parameters are listed:

Parameter	**DQPSK**
N_s (Symbols)	10^6
R_s (GBaud)	25
CPE	**NO CPE**
Pilots (Block Size)	**NO PILOTS**
Laser and LO Linewidth ($\Delta\nu$)	[2; 4] MHz
Frequency Offset (Δf)	[1, 3] GHz
FOC Algorithm	**Spectral Method**

Table 4.5: DQPSK simulation parameters with **phase noise** and **frequency offset**

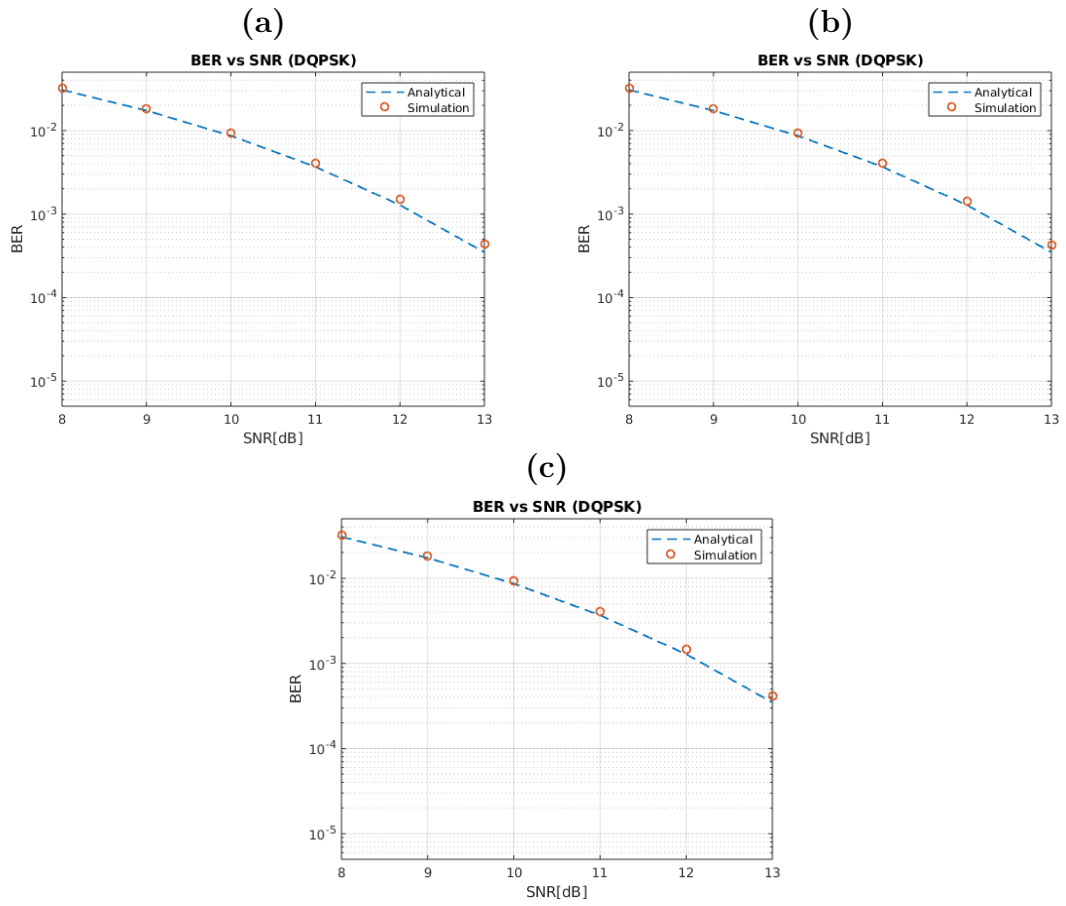

Figure 4.15: BER vs SNR Diagrams (DQPSK)
(a):$\Delta\nu = 2\,\text{MHz},\ \Delta f = 1\,\text{GHz}$
(b):$\Delta\nu = 2\,\text{MHz},\ \Delta f = 2\,\text{GHz}$
(c):$\Delta\nu = 2\,\text{MHz},\ \Delta f = 3\,\text{GHz}$

As in the QPSK case (see Section 4.3.2), DQPSK simulation is carried out fixing linewidth to $\Delta\nu = [2,\ 4]\,\text{MHz}$ and frequency offset between laser and local oscillator changing in the range $\Delta f = [1,\ 3]\,\text{GHz}$. Even here, with $\Delta\nu = 2\,\text{MHz}$ the three BER vs SNR curves are identical each other, and also equal to the case where there is no frequency offset, but only phase noise (Figure 3.5(b)). So, as expected, the used FOC algorithm[8] estimates and compensates correctly with differential modulation format.

[8]The Frequency Offset Compensation algorithm used for simulation is the Spectral Method (Section 4.2.2)

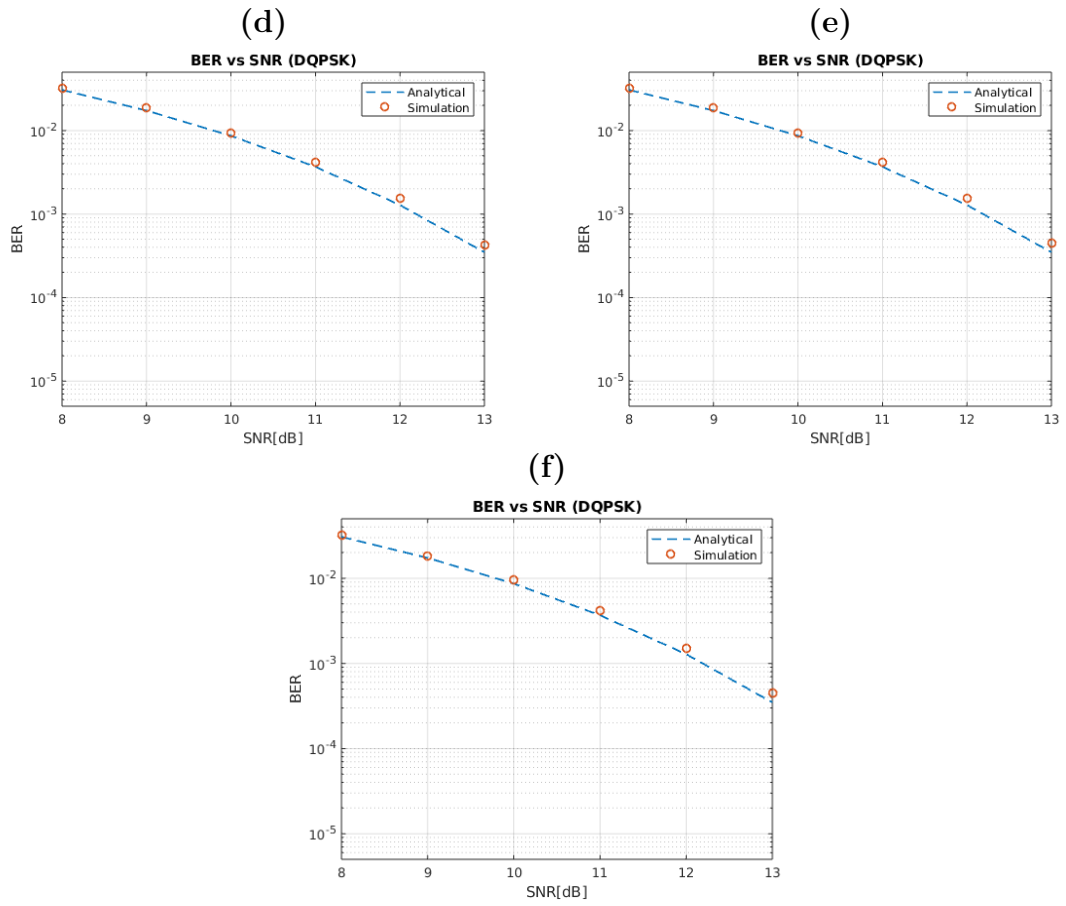

Figure 4.16: BER vs SNR Diagrams (DQPSK)
(d):$\Delta\nu = 4\,\text{MHz},\ \Delta f = 1\,\text{GHz}$
(e):$\Delta\nu = 4\,\text{MHz},\ \Delta f = 2\,\text{GHz}$
(f):$\Delta\nu = 4\,\text{MHz},\ \Delta f = 3\,\text{GHz}$

Increasing laser phase noise ($\Delta\nu = 4\,\text{MHz}$), the outcome does not change. **Frequency offset does not degrade the transmission modulation performances** (see Figure 3.6(d)). Clearly, the previous statement is limited by the implemented FOC algorithm[9]. As it can be seen in Section 4.2.1, Section 4.2.2, Section 4.2.3, they support different estimation ranges.

[9]The Frequency Offset Compensation algorithm used for simulation is the Spectral Method (Section 4.2.2)

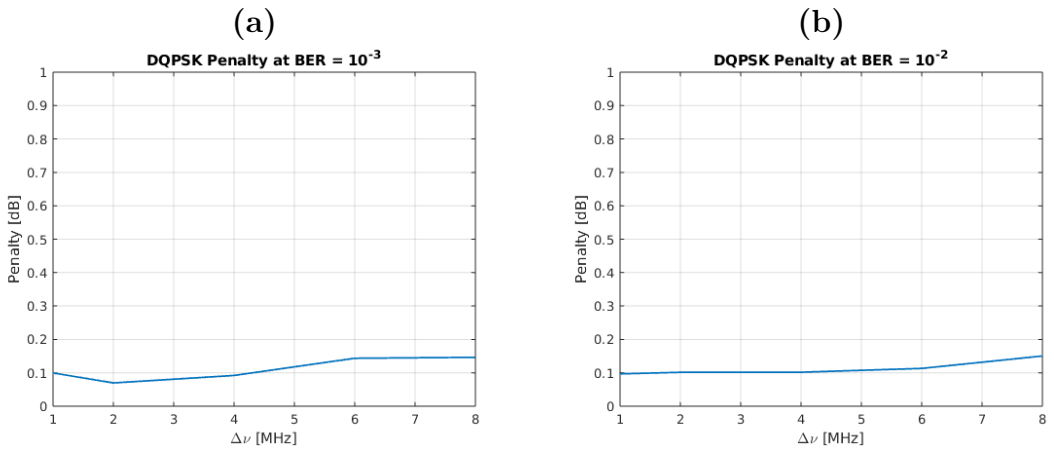

Figure 4.17: DQPSK penalties vs $\Delta\nu$ at BER $= [10^{-3}; 10^{-2}]$ with $\Delta f = 1\,\mathrm{GHz}$

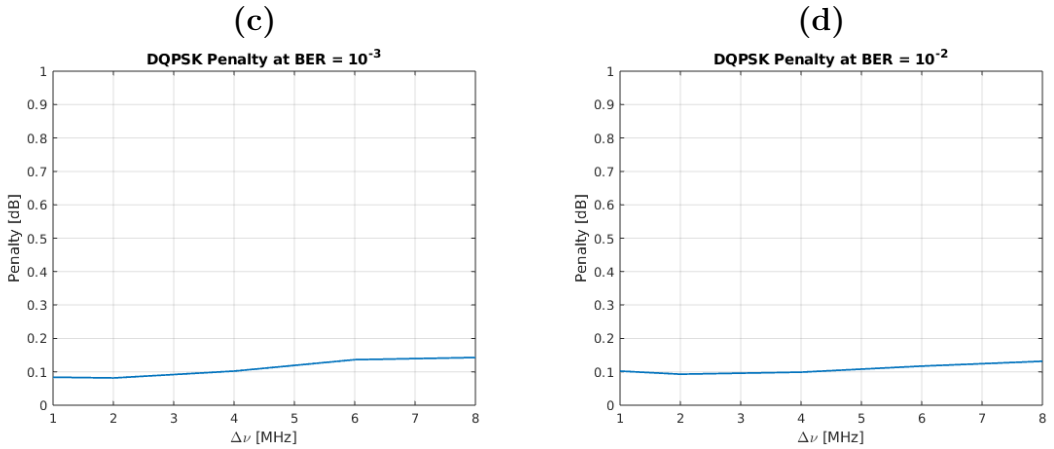

Figure 4.18: DQPSK penalties vs $\Delta\nu$ at BER $= [10^{-3}; 10^{-2}]$ with $\Delta f = 2\,\mathrm{GHz}$

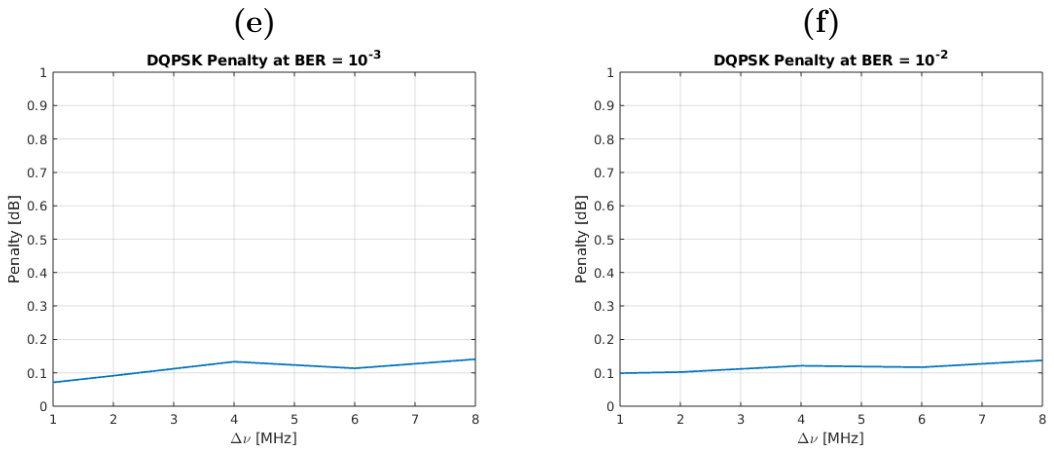

Figure 4.19: DQPSK penalties vs $\Delta\nu$ at BER = $[10^{-3}; 10^{-2}]$ with $\Delta f = 3\,\text{GHz}$

In DQPSK simulation, frequency offset between laser and local oscillator does not affect the estimated penalties. Looking at Section 3.3.2, both penalties (at BER = $[10^{-3}, 10^{-2}]$) [10] are approximately equal. In particular, at $\Delta\nu = 1\,\text{MHz}$, the evaluated penalty is 0.1 dB, while, at $\Delta\nu = 8\,\text{MHz}$, it is 0.15 dB. The shown penalty is only due to the presence of laser phase noise. In fact, if Figure 4.17, Figure 4.18 and Figure 4.19 are compared to Figure 3.7 [11], they almost match. Although the figures exhibit slight variations, they can be considered approximately equal. This similarity arises due to the inherent randomness in different simulation runs, which introduces minor fluctuations but does not significantly affect the overall trend of the results. Finally, the null penalty, due to the frequency offset, is true only if the FOC algorithm is able to estimate the frequency offset with good accuracy.

[10] **These values of BER are evaluated before FEC(Forward Error Correction) codes.** They usually work in a range of BER = $[10^{-3}; 10^{-2}]$. That is why, in the penalty analysis, the focus was on these two specific thresholds.

[11] **$\Delta\nu$ ticks in Figure 4.17, Figure 4.18, Figure 4.19, correspond to the sum of the linewidths of the laser and of the local oscillator** (i.e. $\Delta\nu = 1$ MHz$\rightarrow$ $\Delta\nu_{LAS} = 0.5$ MHz, $\Delta\nu_{LO} = 0.5$ MHz).

4.3.4 Extreme Scenarios

In this paragraph, DQPSK and QPSK simulations are directly compared, including both **laser phase noise** and **frequency offset** between laser and local oscillator. The used DSP receivers are slightly different, given, above all, the CPE block removal. Goal of this Section is to analyze how the two modulation formats behave in very harsh scenarios ($\Delta\nu = [2, 4]\,\text{MHz}$, $\Delta f = 1 \rightarrow 3\,\text{GHz}$), when the optical system is severely affected by impairments which degrade system performances. As a reminder, the main parameters are shown for both versions:

Parameter	**QPSK**	**DQPSK**
N_s (Symbols)	10^6	10^6
R_s (Baud Rate)	25 GBaud	25 GBaud
CPE	$N_{CPE} = 50$ samples	**NO CPE**
Pilots (Block Size)	$Bs_{CPE} = 32$ samples	**NO PILOTS**
Laser and LO Linewidth ($\Delta\nu$)	[2; 4] MHz	[2; 4] MHz
Laser Frequency Offset (Δf)	[1,3] GHz	[1,3] GHz
N_{FOC} (required samples for stable FOC)	10000 samples	5000 samples

Table 4.6: Comparison of QPSK and DQPSK simulation with **PN** and **FO** parameters

The two developed DSP receivers, in particular, have 2 differences. As already mentioned, the one implemented for DQPSK does not have CPE stage with respect to the other one (QPSK), where it is compulsory and furthermore pilots are needed. The second difference regards the Frequency Offset Compensation block. In both dsp receivers, the most stable and robust FOC algorithm is the Spectral Method (see Section 4.2.2). While with QPSK the minimum number of samples needed for a correct FOC is 10000, with DQPSK half of them are enough (5000 samples).

Finally, the whole analysis is carried out in terms of **BER** (BER vs SNR diagram), and **required SNR** (req_snr vs $\Delta\nu$).

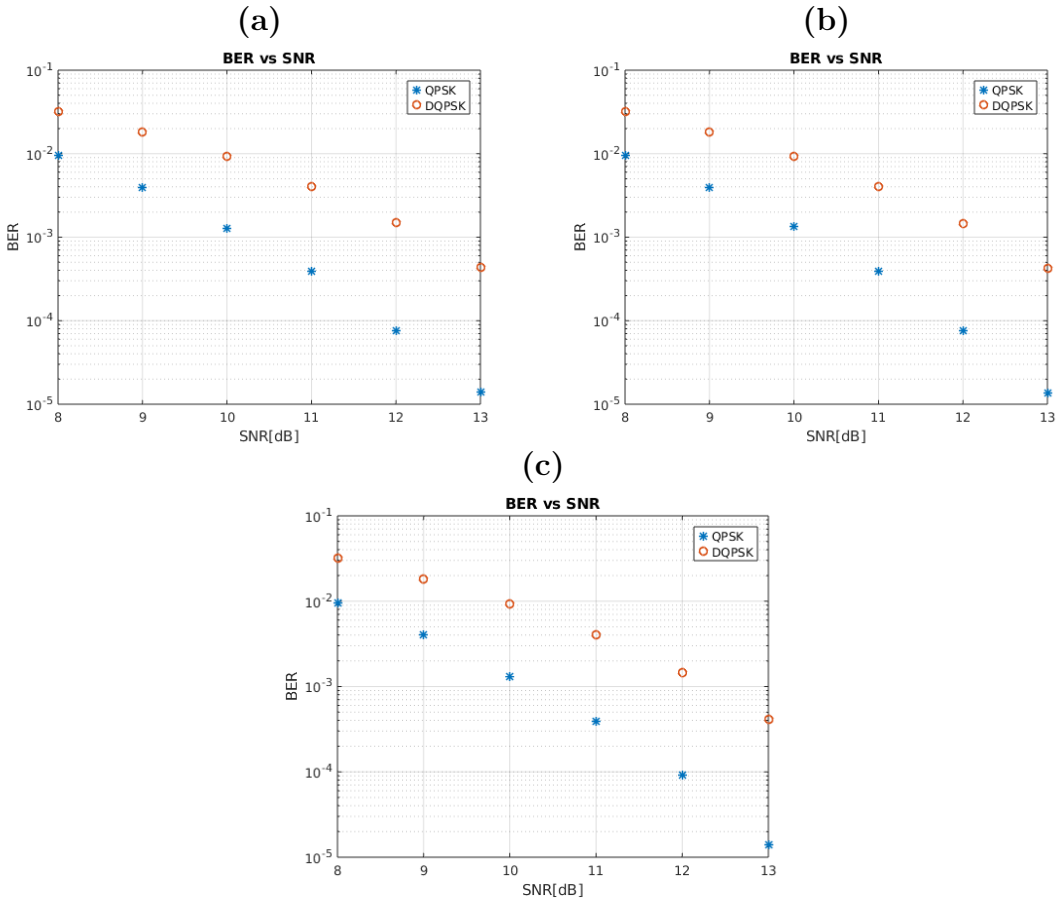

Figure 4.20: BER vs SNR Diagrams (QPSK vs DQPSK)
(a):$\Delta\nu = 2\,\text{MHz}$, $\Delta f = 1\,\text{GHz}$
(b):$\Delta\nu = 2\,\text{MHz}$, $\Delta f = 2\,\text{GHz}$
(c):$\Delta\nu = 2\,\text{MHz}$, $\Delta f = 3\,\text{GHz}$

At a fixed linewidth of $\Delta\nu = 2\,\text{MHz}$, both the QPSK and DQPSK BER vs SNR curves, increasing the frequency offset from 1 to 3 GHz, are not impacted. In other words, the performance loss is caused only by the laser and local oscillator phase noise. Also, another point must be highlighted: DQPSK curve is **always** above the QPSK simulation curve, meaning that in absolute terms, QPSK is better than DQPSK for data transmission.

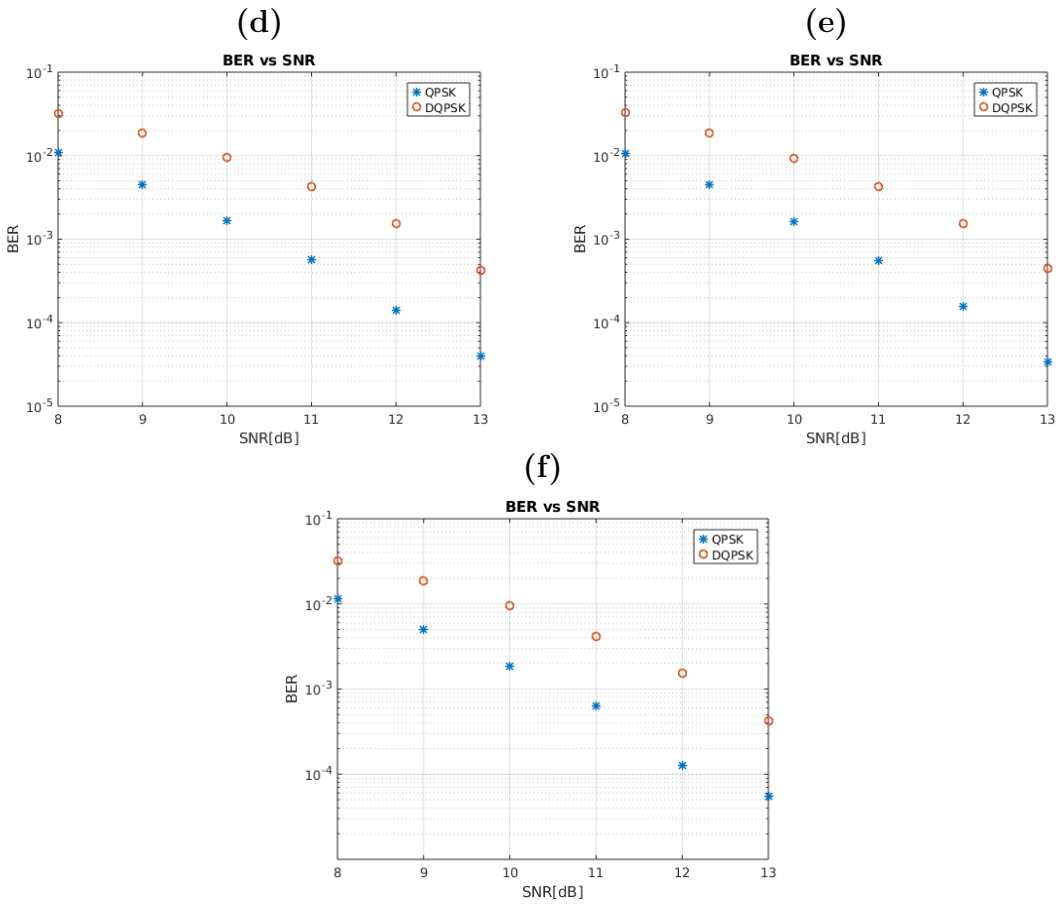

Figure 4.21: BER vs SNR Diagrams (QPSK vs DQPSK)
(d):$\Delta\nu = 4\,\text{MHz}$, $\Delta f = 1\,\text{GHz}$
(e):$\Delta\nu = 4\,\text{MHz}$, $\Delta f = 2\,\text{GHz}$
(f):$\Delta\nu = 4\,\text{MHz}$, $\Delta f = 3\,\text{GHz}$

At $\Delta\nu = 4\,\text{MHz}$, as with $\Delta\nu = 2\,\text{MHz}$, the two simulated curves are not altered by different amounts of frequency offset between laser and local oscillator. Even with such high values of linewidth ($\Delta\nu$) and frequency offset (Δf), QPSK modulation, from a BER point of view, is much better than DQPSK, having lower values of BER for any SNR level. However, looking carefully at Table 4.6, **DQPSK does not need a Carrier Phase Estimation stage** and moreover **only 5000 samples are required to have a perfectly working FOC**. Using QPSK format, instead, **pilots are mandatory in CPE**, because of potential cycle slips, and concerning **FOC block, it needs at least 10000 samples**.

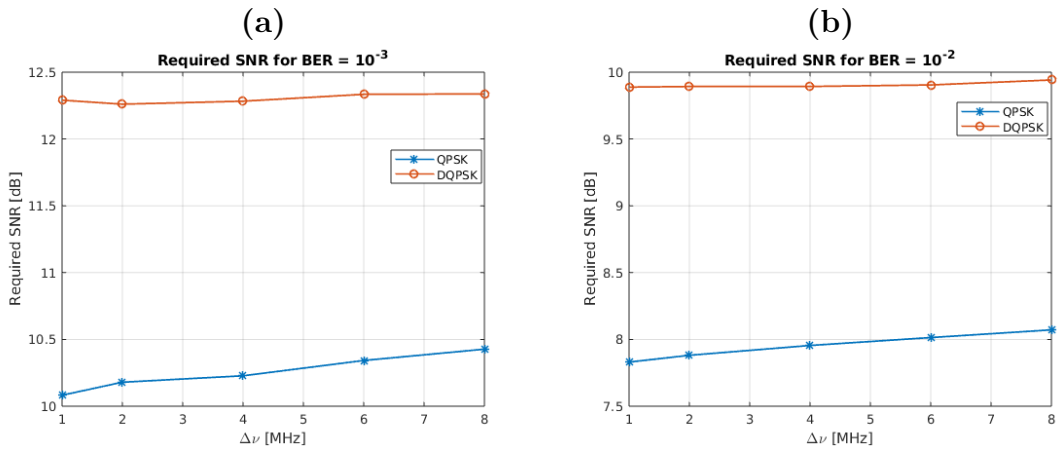

Figure 4.22: Required SNR vs $\Delta\nu$ for BER = $[10^{-3}; 10^{-2}]$ with $\Delta f = 1\,\text{GHz}$

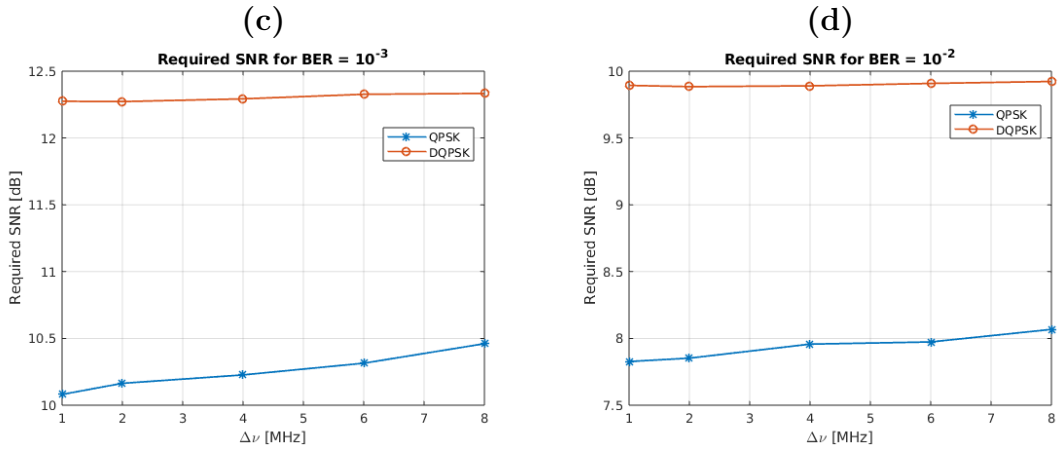

Figure 4.23: Required SNR vs $\Delta\nu$ for BER = $[10^{-3}; 10^{-2}]$ with $\Delta f = 2\,\text{GHz}$

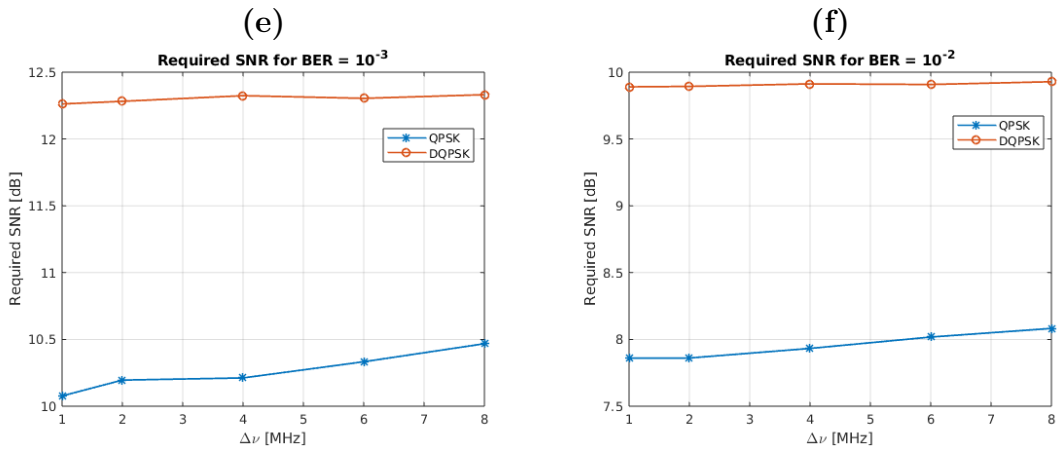

Figure 4.24: Required SNR vs $\Delta\nu$ for BER = $[10^{-3}; 10^{-2}]$ with $\Delta f = 3\,\text{GHz}$

In Figure 4.22, Figure 4.23 and Figure 4.24, the Required SNR vs $\Delta\nu$ results for BER = $[10^{-3}$,$10^{-2}]$ are shown [12]. They help to understand, quantitatively, the overall impact of both the laser and local oscillator phase noise and the frequency offset, between the laser and the local oscillator. In particular, Δf does not affect the required SNR for both BER = $[10^{-3}, 10^{-2}]$. This can be clearly seen comparing each figure of required SNR (Figure 4.22, Figure 4.23, Figure 4.24) with the ones obtained in Chapter 3 (Figure 3.10), where no frequency offset was set. Indeed, they have exactly the same values: for BER = 10^{-3}, at $\Delta\nu = 1$ MHz[13], QPSK has a Required SNR of 10 dB circa while DQPSK 12.2 dB. At $\Delta\nu = 8$ MHz, the Required SNR value of QPSK increases to 10.5 dB, while DQPSK is stable at 12.2 dB. About Required SNR for BER = 10^{-2}, with DQPSK it is constant at a value slightly lower than 10 dB. With QPSK, instead, Required SNR is about 7.8 dB at $\Delta\nu = 1\,\text{MHz}$ and 8.1 dB at $\Delta\nu = 8\,\text{MHz}$. Finally, it is evident the mismatch between the two modulation formats, with QPSK dominating DQPSK.

But, if the metro/access environment is considered, it must take into account the elimination of CPE block with consequently **fully blind dsp receiver** and moreover the **narrower preamble** for Frequency Offset Compensation.

[12]**These values of BER are evaluated before FEC (Forward Error Correction) codes.** They usually work in a range of BER = $[10^{-3}; 10^{-2}]$. That is why, in the penalty analysis, the focus was on these two specific thresholds.

[13]$\Delta\nu$ **ticks in Figure 4.22, Figure 4.23, Figure 4.24, correspond to the sum of the linewidths of the laser and of the local oscillator** (i.e. $\Delta\nu = 1$ MHz$\rightarrow$ $\Delta\nu_{LAS} = 0.5$ MHz, $\Delta\nu_{LO} = 0.5$ MHz).

This outcome is a huge discovery, since with a lower cost, in terms of bits and run time, the system is much more robust to impairments typical of PONs, like laser phase noise and frequency offset.

4.3.5 Convergence Times

Performances, now, are evaluated from another point of view: **Convergence speed**. Goal of this Section is to measure a moving SNR, in order to analyze the transient time (**preamble duration**) after which each system behaves steadily, and consequently is ready to transmit data in an effective way.
To realize these results, the standard SNR formula has been implemented:

$$SNR_{dB} = 10 \cdot log_{10}(\frac{P_{TX}}{\sigma_n^2}) = 10 \cdot log_{10}(\frac{P_{RX} - \sigma_n^2}{\sigma_n^2})$$

where:

- P_{RX} is the power of the received signal y_{RX}
- σ_n^2 is the noise variance, which corresponds to the noise power

But, since the focus is on the behavior of SNR along the time (samples), a **moving SNR** has been implemented, where the noise variance is computed **over a sliding window of 50 samples**. In particular, the two modulation formats are studied under 3 levels of noise, **using an AWGN channel in the Channel block**: $SNR_{AWGN} = [8 \text{ dB (high noise)}, 10 \text{ dB (medium noise)}, 12 \text{ dB (low noise)}]$ (Figure 4.25, Figure 4.26, Figure 4.27).

In this scenario, regarding linewidth and frequency offset, the selected values are:$\Delta\nu = 4\,\text{MHz}$, $\Delta f = 3\,\text{GHz}$.

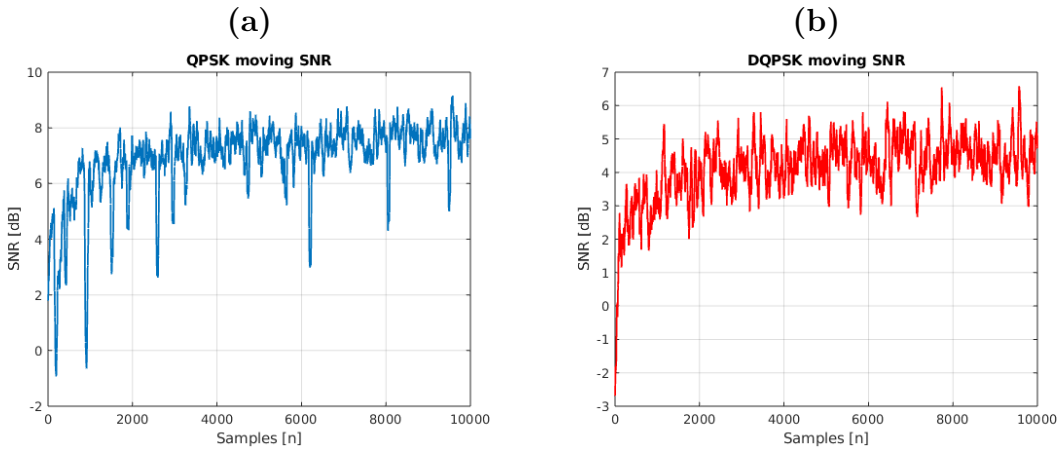

Figure 4.25: Estimated SNR for QPSK**(a)** and DQPSK**(b)** at **SNR = 8 dB**

For a high quantity of noise (SNR = 8 dB), with both QPSK and DQPSK(Figure 4.25), DSP receiver starts to converge after 2000 samples ca. . The curves are

really similar each other, except for one feature. Although both of them oscillate approximately ±1 dB around the middle point (7.5 dB for QPSK, 4.5 dB for DQPSK), the QPSK moving SNR present dips of more than 3 dB. These drops are caused by **cycle slips**. A cycle slip occurs when the phase of a received signal suddenly jumps by a multiple of $\frac{2\pi}{M}$ (for a M-PSK system, such as QPSK where N=4). This happens due to high quantity of laser phase noise, and low SNR conditions. When a cycle slip happens, the demodulator momentarily loses phase synchronization, leading to **bit errors and a sudden drop in the SNR**. In order to recover the phase synchronization, **QPSK needs pilots**. If the interested region is zoomed in, it is possible to see that **they have a length duration of 32 samples**, which is the pilots separation. Obviously, those samples will be discarded.
Furthermore there is a great difference between QPSK and DQPSK: the y-scale. In every couple of figures, moving SNR of QPSK is always higher than DQPSK of about 3 dB. This result is because of how SNR has been evaluated. In fact, in the DQPSK system, before to estimate SNR the differential encoded signal is decoded into a QPSK format, and this introduces an inherent 3 dB penalty due to the differential decoding process, which results in a reduced SNR compared to the QPSK format.

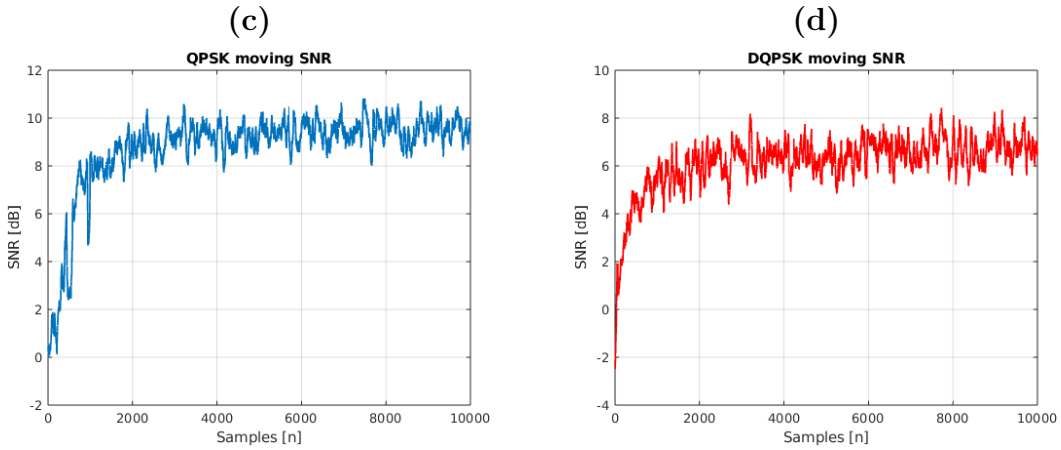

Figure 4.26: Estimated SNR for QPSK**(c)** and DQPSK**(d)** at **SNR = 10 dB**

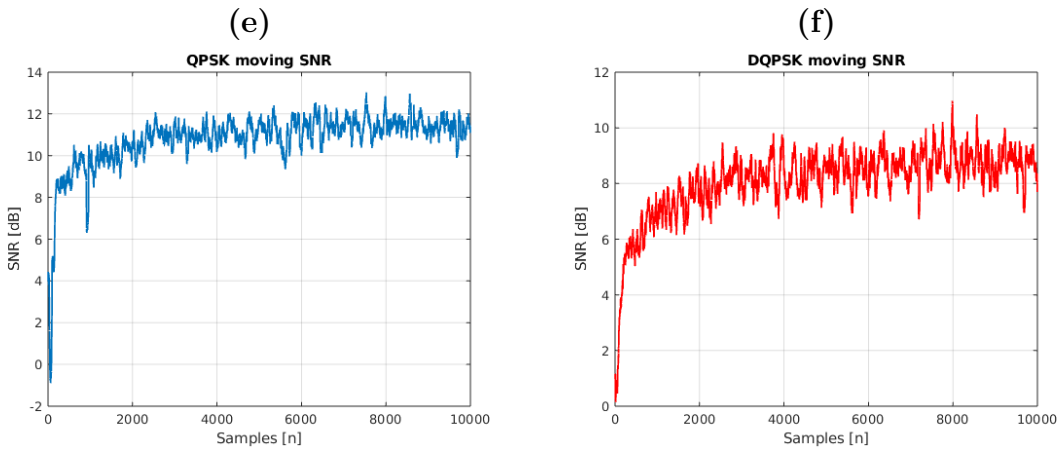

Figure 4.27: Estimated SNR for QPSK**(e)** and DQPSK**(f)** at **SNR = 12 dB**

At medium and low level of noise (Figure 4.26, Figure 4.27), the transient duration is similar to the previous case (2000 samples). In Figure 4.26(c) and Figure 4.27(e), there are still some SNR dips, but they occur primarily in the transient region, which is expected and acceptable since the system has not fully converged yet, and consequently the samples would be discarded anyway.
The goal of this Section is to analyze how the SNR of QPSK and DQPSK evolves over time, highlighting the trade-off between transmission quality and the number of usable samples.

Chapter 5

Conclusions and Future Work

This work proposes a possible future solution for metro/access coherent passive optical networks (PONs). The growing demand for high bandwidth per user is making **Intensity Modulation with Direct Detection (IMDD)** technology insufficient, despite its widespread adoption in PONs. The first step toward addressing this challenge is the transition from IMDD to coherent detection, which enables the use of advanced modulation formats (e.g., M-PSK, M-QAM) with significantly higher spectral efficiency.

A key advantage of coherent technology over IMDD in passive optical networks (PONs) is its improved sensitivity and spectral efficiency. Unlike IMDD-PON, which relies on direct detection and is limited by lower receiver sensitivity and dispersion tolerance, Coherent-PON enables higher data rates and longer reach by leveraging coherent detection and digital signal processing (DSP). This allows for more efficient frequency offset compensation (FOC) and carrier phase estimation (CPE), resulting in superior performance in terms of **optical power budget** and **reach** [4]-[5].

The transition to coherent detection in metro/access networks is inspired by its successful deployment in long-haul optical communication systems. However, due to the **high cost and energy consumption** associated with conventional coherent technology, its direct application to PONs is not feasible for telecom operators. To address this limitation, a simplified version of coherent detection is proposed, where the DSP algorithms are optimized for lower complexity, and certain impairments such as fiber non-linearities, which are negligible in short-reach systems, are not considered. This streamlined approach, referred to as **Lite Coherent**, retains only

the essential processing required to mitigate impairments typical of metro/access networks while significantly reducing cost and power consumption compared to traditional coherent systems.

The results presented in Chapters 3 and 4 evaluate two modulation formats: **QPSK and DQPSK**. QPSK is widely adopted in optical networks, while DQPSK is explored in this work as a potential alternative. **Bit Error Rate (BER) performance** analysis across different **Signal-to-Noise Ratio (SNR)** levels indicates that QPSK outperforms DQPSK under ideal conditions. However, this performance gap is reduced in the presence of impairments. Specifically, while DQPSK inherently suffers a **3 dB penalty** compared to QPSK, it exhibits greater robustness against **laser phase noise and frequency offset**. As a result, the BER penalty between QPSK and DQPSK is reduced to **1.5–2 dB** under realistic conditions.

A primary objective of this study is to explore an alternative to QPSK while **simplifying the DSP receiver structure** to develop a low-cost solution. Given its increased resilience to impairments, DQPSK is a promising candidate, particularly for **low-maintenance optical networks**, such as those in central offices or regions where **cost-effective, high-linewidth lasers** are preferable. Another key advantage of DQPSK is its compatibility with a **fully blind DSP receiver**, eliminating the need for carrier phase estimation (CPE) and thus further simplifying the receiver architecture.

Finally, in order to enhance and validate the proposed **DQPSK Lite Coherent system** further research efforts can be delivered toward experimental tests. In fact, the current results are based on **MATLAB simulations**, which offer valuable insights but may not fully reflect real-world conditions. A natural next step is to implement and test the proposed DSP receiver in a physical optical network. Experimental validation would help refine the algorithms, address practical implementation challenges, and ensure the technology's feasibility for deployment in metro/access scenarios.

List of Tables

2.1 QPSK Symbol Mapping 6
2.2 DQPSK Symbol Mapping 7

3.1 QPSK simulation parameters with only **phase noise** 18
3.2 DQPSK simulation parameters with only **phase noise** 21
3.3 Comparison of QPSK and DQPSK simulation parameters 24

4.1 FOC Algorithms Comparison in different scenarios (QPSK) 36
4.2 FOC Algorithms Comparison in different scenarios (DQPSK) 36
4.3 FOC Algorithms Complexity 37
4.4 QPSK simulation parameters with **phase noise** and **frequency offset** 38
4.5 DQPSK simulation parameters with **phase noise** and **frequency offset** 43
4.6 Comparison of QPSK and DQPSK simulation with **PN** and **FO** parameters 48

List of Figures

2.1 QPSK Constellation 6
2.2 DQPSK Constellation 7
2.3 Comparison of BER vs SNR Analytical Curves between QPSK and DQPSK 9
2.4 Transmitter Block 10
2.5 Channel Block 11
2.6 Receiver Block 12
2.7 Downsampled Signal 13

3.1 Basic phase estimator for m-PSK carriers [7] 17
3.2 BER vs SNR Diagrams (QPSK)[**(a)**: $\Delta\nu = 1\,\text{MHz}$, **(b)**: $\Delta\nu = 2\,\text{MHz}$] 19
3.3 BER vs SNR Diagrams (QPSK)[**(c)**: $\Delta\nu = 3\,\text{MHz}$, **(d)**: $\Delta\nu = 4\,\text{MHz}$] 19
3.4 QPSK penalties vs $\Delta\nu$ at BER = $[10^{-3}; 10^{-2}]$ 20
3.5 BER vs SNR Diagrams (DQPSK)[**(a)**:$\Delta\nu = 1\,\text{MHz}$, **(b)**:$\Delta\nu = 2\,\text{MHz}$] 21
3.6 BER vs SNR Diagrams (DQPSK)[**(c)**:$\Delta\nu = 3\,\text{MHz}$, **(d)**:$\Delta\nu = 4\,\text{MHz}$] 22
3.7 DQPSK penalties vs $\Delta\nu$ at BER = $[10^{-3}; 10^{-2}]$ 23
3.8 BER vs SNR Diagrams (QPSK vs DQPSK)[**(a)**:$\Delta\nu = 1\,\text{MHz}$, **(b)**:$\Delta\nu = 2\,\text{MHz}$] 24
3.9 BER vs SNR(QPSK vs DQPSK)[**(c)**:$\Delta\nu = 3\,\text{MHz}$, **(d)**:$\Delta\nu = 4\,\text{MHz}$] 25
3.10 Required SNR vs $\Delta\nu$ for BER = $[10^{-3}; 10^{-2}]$ 26

4.1 Block diagram of the frequency estimator 28
4.2 Block diagram of the algorithm. (a)Frequency estimator by employing FFT; (b) the whole structure of the algorithm [15]. 29
4.3 Differential Phase-Based Method convergence time(QPSK) [$\Delta\nu = 500\,\text{KHz}$, $\Delta f = 1.5\,\text{GHz}$] 31

4.4 FOC Convergence Times (QPSK)
(a):$\Delta\nu = 500\,\text{kHz}$, $\Delta f = 3\,\text{GHz}$ **(b)**:$\Delta\nu = 500\,\text{kHz}$, $\Delta f = 3\,\text{GHz}$
(c):$\Delta\nu = 500\,\text{kHz}$, $\Delta f = 3\,\text{GHz}$ 32
4.5 FOC Convergence Times (DQPSK)
(d):$\Delta\nu = 500\,\text{kHz}$, $\Delta f = 3\,\text{GHz}$ **(e)**:$\Delta\nu = 500\,\text{kHz}$, $\Delta f = 3\,\text{GHz}$
(f):$\Delta\nu = 500\,\text{kHz}$, $\Delta f = 3\,\text{GHz}$ 33
4.6 Power Spectral Density (PSD) of QPSK signal
(a): at equalizer input **(b)**: at equalizer output 34
4.7 Power Spectral Density (PSD) of DQPSK signal
(c): at equalizer input **(d)**: at equalizer output 34
4.8 FOC Convergence Times (QPSK)
(a):$\Delta\nu = 4\,\text{MHz}$, $\Delta f = 3\,\text{GHz}$ **(b)**:$\Delta\nu = 4\,\text{MHz}$, $\Delta f = 3\,\text{GHz}$ . . . 35
4.9 FOC Convergence Times (DQPSK)
(c):$\Delta\nu = 4\,\text{MHz}$, $\Delta f = 3\,\text{GHz}$ **(d)**:$\Delta\nu = 4\,\text{MHz}$, $\Delta f = 3\,\text{GHz}$ . . . 35
4.10 BER vs SNR Diagrams (QPSK)
(a):$\Delta\nu = 2\,\text{MHz}$, $\Delta f = 1\,\text{GHz}$ **(b)**:$\Delta\nu = 2\,\text{MHz}$, $\Delta f = 2\,\text{GHz}$
(c):$\Delta\nu = 2\,\text{MHz}$, $\Delta f = 3\,\text{GHz}$ 39
4.11 BER vs SNR Diagrams (QPSK)
(d):$\Delta\nu = 4\,\text{MHz}$, $\Delta f = 1\,\text{GHz}$ **(e)**:$\Delta\nu = 4\,\text{MHz}$, $\Delta f = 2\,\text{GHz}$
(f):$\Delta\nu = 4\,\text{MHz}$, $\Delta f = 3\,\text{GHz}$ 40
4.12 QPSK penalties vs $\Delta\nu$ at BER = $[10^{-3}; 10^{-2}]$ with $\Delta f = 1\,\text{GHz}$ . . 41
4.13 QPSK penalties vs $\Delta\nu$ at BER = $[10^{-3}; 10^{-2}]$ with $\Delta f = 2\,\text{GHz}$ . . 41
4.14 QPSK penalties vs $\Delta\nu$ at BER = $[10^{-3}; 10^{-2}]$ with $\Delta f = 3\,\text{GHz}$ . . 42
4.15 BER vs SNR Diagrams (DQPSK)
(a):$\Delta\nu = 2\,\text{MHz}$, $\Delta f = 1\,\text{GHz}$ **(b)**:$\Delta\nu = 2\,\text{MHz}$, $\Delta f = 2\,\text{GHz}$
(c):$\Delta\nu = 2\,\text{MHz}$, $\Delta f = 3\,\text{GHz}$ 44
4.16 BER vs SNR Diagrams (DQPSK)
(d):$\Delta\nu = 4\,\text{MHz}$, $\Delta f = 1\,\text{GHz}$ **(e)**:$\Delta\nu = 4\,\text{MHz}$, $\Delta f = 2\,\text{GHz}$
(f):$\Delta\nu = 4\,\text{MHz}$, $\Delta f = 3\,\text{GHz}$ 45
4.17 DQPSK penalties vs $\Delta\nu$ at BER = $[10^{-3}; 10^{-2}]$ with $\Delta f = 1\,\text{GHz}$. 46
4.18 DQPSK penalties vs $\Delta\nu$ at BER = $[10^{-3}; 10^{-2}]$ with $\Delta f = 2\,\text{GHz}$. 46
4.19 DQPSK penalties vs $\Delta\nu$ at BER = $[10^{-3}; 10^{-2}]$ with $\Delta f = 3\,\text{GHz}$. 47
4.20 BER vs SNR Diagrams (QPSK vs DQPSK)
(a):$\Delta\nu = 2\,\text{MHz}$, $\Delta f = 1\,\text{GHz}$ **(b)**:$\Delta\nu = 2\,\text{MHz}$, $\Delta f = 2\,\text{GHz}$
(c):$\Delta\nu = 2\,\text{MHz}$, $\Delta f = 3\,\text{GHz}$ 49
4.21 BER vs SNR Diagrams (QPSK vs DQPSK)
(d):$\Delta\nu = 4\,\text{MHz}$, $\Delta f = 1\,\text{GHz}$ **(e)**:$\Delta\nu = 4\,\text{MHz}$, $\Delta f = 2\,\text{GHz}$
(f):$\Delta\nu = 4\,\text{MHz}$, $\Delta f = 3\,\text{GHz}$ 50
4.22 Required SNR vs $\Delta\nu$ for BER = $[10^{-3}; 10^{-2}]$ with $\Delta f = 1\,\text{GHz}$ . . 51
4.23 Required SNR vs $\Delta\nu$ for BER = $[10^{-3}; 10^{-2}]$ with $\Delta f = 2\,\text{GHz}$ . . 51
4.24 Required SNR vs $\Delta\nu$ for BER = $[10^{-3}; 10^{-2}]$ with $\Delta f = 3\,\text{GHz}$ . . 52

4.25 Estimated SNR for QPSK(**a**) and DQPSK(**b**) at **SNR = 8 dB** . . 54
4.26 Estimated SNR for QPSK(**c**) and DQPSK(**d**) at **SNR = 10 dB** . 55
4.27 Estimated SNR for QPSK(**e**) and DQPSK(**f**) at **SNR = 12 dB** . 56

Bibliography

[1] G. Kramer. *Ethernet Passive Optical Networks*. Professional Engineering. McGraw Hill LLC, 2005. Chap. 8. ISBN: 9780071466400. URL: https://books.google.it/books?id=leTxSysNE_kC (cit. on p. 1).

[2] Haipeng Zhang, Zhensheng (Steve) Jia, and L. Alberto Campos. «Unleashing the Power of Coherent Optical Technology». In: *NCTA Technical Papers*. 2024. URL: https://www.nctatechnicalpapers.com/Paper/2024/WLINE09_Zhang_6544_paper (cit. on p. 1).

[3] Jayant Baliga, Robert Ayre, Kerry Hinton, and Rodney S. Tucker. «Energy consumption in wired and wireless access networks». In: *IEEE Communications Magazine* 49.6 (2011), pp. 70–77. DOI: 10.1109/MCOM.2011.5783987 (cit. on p. 1).

[4] Ji Zhou et al. «Flexible Coherent Optical Access: Architectures, Algorithms, and Demonstrations». In: *Journal of Lightwave Technology* 42.4 (2024), pp. 1193–1202. DOI: 10.1109/JLT.2024.3355443 (cit. on pp. 2, 57).

[5] Haipeng Zhang, Zhensheng Jia, Luis Alberto Campos, and Curtis Knittle. «Experimental Demonstration of Rate-Flexible Coherent PON Up to 300 Gb/s». In: *Journal of Lightwave Technology* 42.16 (2024), pp. 5440–5449. DOI: 10.1109/JLT.2024.3366163 (cit. on pp. 2, 57).

[6] Vincent Houtsma and Dora van Veen. «Higher-speed PONs based on data center technology and optics [Invited]». In: *Journal of Optical Communications and Networking* 16.2 (2024), A98–A104. DOI: 10.1364/JOCN.501410 (cit. on p. 2).

[7] Andrew J. Viterbi and Audrey M. Viterbi. «Nonlinear estimation of PSK-modulated carrier phase with application to burst digital transmission». In: *IEEE Trans. Inf. Theory* 29.4 (1983), pp. 543–550. DOI: 10.1109/TIT.1983.1056713. URL: https://doi.org/10.1109/TIT.1983.1056713 (cit. on pp. 8, 14, 17).

[8] Proakis. *Digital Communications 5th Edition*. McGraw Hill, 2007, p. 195 (cit. on p. 8).

[9] Kazuro Kikuchi. «Fundamentals of Coherent Optical Fiber Communications». In: *Journal of Lightwave Technology* 34.1 (2016), pp. 157–179. DOI: 10.1109/JLT.2015.2463719 (cit. on p. 12).

[10] Seb J. Savory. «Digital Coherent Optical Receivers: Algorithms and Subsystems». In: *IEEE Journal of Selected Topics in Quantum Electronics* 16 (2010), pp. 1164–1179. URL: https://api.semanticscholar.org/CorpusID:22913763 (cit. on pp. 12, 17, 28).

[11] Hans Wenzel, Markus Kantner, Mindaugas Radziunas, and Uwe Bandelow. «Semiconductor Laser Linewidth Theory Revisited». In: *Applied Sciences* 11.13 (June 2021), p. 6004. ISSN: 2076-3417. DOI: 10.3390/app11136004. URL: http://dx.doi.org/10.3390/app11136004 (cit. on p. 14).

[12] Thorlabs. *Single-Frequency Lasers Tutorial*. Year. URL: https://www.thorlabs.com/newgrouppage9.cfm?objectgroup_id=9024 (cit. on p. 16).

[13] Andreas Leven, Noriaki Kaneda, Ut-Va Koc, and Young-Kai Chen. «Frequency Estimation in Intradyne Reception». In: *Photonics Technology Letters, IEEE* 19 (Apr. 2007), pp. 366–368. DOI: 10.1109/LPT.2007.891893 (cit. on p. 28).

[14] Sebastian Hoffmann, Suhas Bhandare, Timo Pfau, Olaf Adamczyk, Christian Wordehoff, Ralf Peveling, Mario Porrmann, and Reinhold Noe. «Frequency and Phase Estimation for Coherent QPSK Transmission With Unlocked DFB Lasers». In: *IEEE Photonics Technology Letters* 20.18 (2008), pp. 1569–1571. DOI: 10.1109/LPT.2008.928846 (cit. on p. 28).

[15] Yinwen Cao, Song Yu, Jing Shen, Wanyi Gu, and Yuefeng Ji. «Frequency Estimation for Optical Coherent MPSK System Without Removing Modulated Data Phase». In: *IEEE Photonics Technology Letters* 22.10 (2010), pp. 691–693. DOI: 10.1109/LPT.2010.2044170 (cit. on p. 29).

[16] Yumin Liu, Yunfeng Peng, Shuang Wang, and Zonglong Chen. «Improved FFT-Based Frequency Offset Estimation Algorithm for Coherent Optical Systems». In: *IEEE Photonics Technology Letters* 26.6 (2014), pp. 613–616. DOI: 10.1109/LPT.2014.2301796 (cit. on p. 29).